An Observational History of the Direct Influence of the Stratospheric Quasi-biennial Oscillation on the Tropical and Subtropical Upper Troposphere and Lower Stratosphere

Matthew H. HITCHMAN[1]
Department of Atmospheric and Oceanic Sciences
University of Wisconsin – Madison, Madison, WI, USA

Shigeo YODEN
Institute for Liberal Arts and Sciences and Graduate School of Geoscience
Kyoto University, Kyoto, Japan

Peter H. HAYNES
Department of Applied Mathematics and Theoretical Physics
Cambridge University, Cambridge, United Kingdom

Vinay KUMAR
Radio and Atmospheric Physics Lab, Rajdhani College
University of Delhi, Delhi, India

Susann TEGTMEIER
Department of Physics and Engineering Physics
University of Saskatchewan, Saskatoon, Canada

Submitted April 30, 2020; Revised August 5, 2020; October 7, 2020; November 2, 2020

---

1) Corresponding Author: Matthew H. Hitchman, Department of Atmospheric and Oceanic Sciences, 1225 West Dayton Street, University of Wisconsin – Madison, Madison, WI, 53706, USA.
Email: matt@aos.wisc.edu
Tel: 1- 608-262-4653

Fax: 1-608-262-0166

Abstract

The history of observational studies regarding the influence of the stratospheric quasi-biennial oscillation (QBO) on the tropical and subtropical upper troposphere and lower stratosphere (UTLS) is reviewed. QBO westerly (W) and easterly (E) phases are defined by zonal winds in the lower stratosphere. During 1960-1978, radiosonde data revealed a QBO modulation of the UTLS, with a warm anomaly during QBO W in the tropics, and cool anomalies near 30°S and 30°N. This agreed with theory of the QBO mean meridional circulation (MMC), which predicted a coherent, anti-phased response between the tropics and subtropics. During 1978-1994, satellite observations of aerosol and temperature confirmed the existence of the QBO MMC. During 1994-2001, global data sets enabled analysis of zonal mean QBO variations in tropopause temperature. In 2001, National Centers for Environmental Prediction reanalyses for the 42-yr period 1958-2000 revealed seasonal and geographical variations in QBO W-E tropopause temperature, pressure, and zonal wind, which are presented here. An update using the 38-yr Modern-Era Retrospective analysis for Research and Applications, Version 2 and 40-yr European Centre for Medium Range Weather Forecasting Reanalysis -Interim data sets provides a more complete view of seasonal and geographical variation.

The QBO range in tropical tropopause values is ~0.5-2 K, ~100-300 m, and ~1-3 hPa, being colder and higher during QBO E, especially during boreal winter and spring. The QBO temperature signal tends to be larger near regions where deep convection is common. The QBO signal in the southern subtropics is enhanced during austral winter. During QBO W, the subtropical westerly jet is enhanced, while the Walker circulation is weaker, especially during boreal spring. A new climatology of zonal mean QBO anomalies in temperature, zonal wind,

and MMC is presented. QBO E may enhance convection by reducing both static stability and wind shear in the UTLS.

Keywords: quasi-biennial oscillation; tropopause; tropics; subtropics; general circulation

1. Introduction

The westward progression of orange sunsets around the globe in the tropics after the eruption of Krakatau in August 1883 showed that there was a layer of easterly (E) winds in the tropical stratosphere at that time (Simkin and Fiske 1984; Winchester 2003; Hamilton 2012). In August 1908, Berson (1910) found a thin layer of westerly (W) winds in pilot balloon observations over tropical Africa, underlying a layer of easterly winds. This view of a layered structure, with "Krakatau easterlies" overlying a thin layer of "Berson westerlies" prevailed for fifty years (Hastenrath 2007; Brönniman and Stickler 2013), until several consecutive years of tropical radiosonde data were analyzed by Reed et al. (1961) and Veryard and Ebdon (1961). These papers reported the discovery of the stratospheric quasi-biennial oscillation (QBO), wherein alternating layers of W and E winds descend in the stratosphere at ~ 1 km/mo., and diminish in amplitude approaching the upper troposphere / lower stratosphere (UTLS), exhibiting a variable periodicity of ~24-32 months (Fig. 1).

The QBO is primarily driven by vertical momentum fluxes due to upward-propagating equatorial wave activity, which are generated by tropospheric convective systems (Andrews et al. 1987). Another wave driving contribution comes from the meridional momentum flux convergence associated with extratropical planetary waves (Dunkerton 1983). Usually this process is not as important as tropical wave driving, but it has been shown to be a likely cause

for the disruption of descending QBO westerlies during 2015/2016 (Osprey et al. 2016, Newman et al. 2016, Coy et al. 2017).

An overview of the QBO is provided by Baldwin et al. (2001). The focus of the present historical review is on observational studies of QBO effects in the UTLS in the tropics and subtropics, including the tropical tropopause layer (TTL). Gettelman and Forster (2002) suggested that the TTL extends from the level of lapse rate minimum at 10–12 km to the mean cold point tropopause (CPT) level at 17 km or 90 hPa. Fueglistaler et al. (2009) analyzed a range of meteorological and constituent data and suggested a working definition of the TTL as the 14-18.5 km layer (150-70 hPa or 355-425 K layer). Since the QBO MMC extends into the subtropics and upward into the stratosphere, the term UTLS will be used to indicate the tropical and subtropical upper troposphere and lower stratosphere.

Since the discovery of the QBO, observational studies have revealed interesting correlations between the QBO and other phenomena, including an anti-phased relationship between the tropical and subtropical lower stratosphere (Angell and Korshover 1964) and modulation of the tropical tropopause altitude (Reid and Gage 1985). Evidence also emerged that the QBO influences the winter polar vortex, where QBO E favors a more disturbed polar vortex (Holton and Tan 1980). Anstey and Shepherd (2014) provide a comprehensive review of studies of the "Holton-Tan effect". Boville (1984), Baldwin and Dunkerton (1999), Thompson and Wallace (2001), and others have shown that the state of the extratropical stratosphere can modulate extratropical tropospheric weather patterns. This constitutes an extratropical stratosphere – troposphere coupling pathway, whereby the QBO can influence tropospheric weather via the extratropical stratosphere.

An evaluation of global reanalyses of the QBO signal in zonal wind is given by Kawatani et al. (2016). A summary of global surface impacts of the QBO is given by Gray et al. (2018). Attard and Coy (2019) discuss QBO effects on the polar winter stratosphere. Chapter 9 of Anstey et al. (2020, in preparation) presents an archive of figures regarding QBO variability in the tropics, for an array of global reanalysis data sets analyzed for the Stratosphere-troposphere Processes and their Role in Climate (SPARC) Reanalysis Intercomparison Project (S-RIP). Haynes et al. (2020) provide an overview of theoretical and modeling aspects of the coupling between the stratosphere and troposphere involving the QBO, including a discussion of the interaction between the QBO and the Madden Julian Oscillation (MJO).

The present review focuses on the history of observationally-based studies regarding the direct influence of the QBO on the tropical and subtropical UTLS. The primary purpose here is to describe significant relationships seen in the observations. An assessment of possible mechanisms, evaluated for consistency with the observed geographical distribution of the QBO signal in the UTLS, is given near the end. This history is described sequentially, according to stages of development in instrumental and global analysis capabilities. During 1960-1978, radiosonde data provided the first observations of QBO effects in the tropical and subtropical UTLS, with simultaneous development of a theoretical description of the QBO MMC as a wave-driven circulation. During 1978-1994, new satellite observations of volcanic aerosol and temperature provided information which supported the theoretical structure of the QBO MMC. During 1994-2001, development of global data sets allowed for new estimations of the zonal mean QBO in tropopause temperature, highlighting the latitudinal anti-phased nature and effect across the UTLS.

In the early 2000s, data from the National Centers for Environmental Prediction (NCEP) for the period 1958-2000 were used by the lead author (MHH) to investigate the seasonal and geographical variation of the QBO signal in the tropical and subtropical TTL. Results were presented orally at five international scientific meetings during 2000-2003, including the SPARC 2nd General Assembly, Mar del Plata, Argentina (2000, 6-10 November), the JSPS/NSF Japan - U.S. Seminar on Coupling of the Troposphere and Stratosphere by Dynamical, Radiative and Chemical Processes, Kyoto, Japan (2001, 13-17 March), the Risk Prediction Initiative Conference on Forecasting Severe Weather in Bermuda (2002), the AMS 12th Conference on Middle Atmosphere, San Antonio, USA (2002, 4-7 November), and the SPARC Workshop on the Role of the Stratosphere in Tropospheric Climate, Whistler BC, Canada (2003, 29 April - 2 May). Three of these figures are included as historical Figs. 14-16 in this paper. At the time, the primary focus regarding QBO influences on the troposphere was on the Holton-Tan effect. Although the idea of a "direct effect" of the QBO on the tropical and subtropical UTLS had been discussed in the literature since the 1960s, in the early 2000s it was not yet widely accepted. Presentation of these figures eventually helped to generate interest in the possibility that there are geographical variations in the QBO signal in the tropics. During 2015-2019, the second author (SY) re-invigorated interest in the direct effect of the QBO on tropical convection by organizing a series of workshops in Japan. The lead author gave six presentations on this topic during 2015-2020.

Now it is possible to compare the geographical and seasonal variation in the QBO signal in the deep tropics in the 2001 NCEP study with results using CPT temperatures from Modern-Era Retrospective Analysis for Research and Applications, Version 2 (MERRA-2) data for the 38-yr period 1980-2017, and with results from European Centre for Medium Range Weather

147 Forecasting Reanalysis (ERA-Interim) data from the 40-yr period 1979-2018. These modern
148 data sets extend the observational record by almost two decades. Further analysis of ERA-
149 Interim data enables a more comprehensive description of the seasonal and geographical
150 variations in the QBO signal in the tropical and subtropical UTLS, and provides a new depiction
151 of the QBO anomalies in zonal wind, temperature, and MMC in the region 1000-1 hPa, 40°S-
152 40°N.

153 Data and analysis methods for the NCEP, MERRA-2 and ERA-Interim data sets are
154 described in Section 2, including discussion of QBO indices and statistical significance testing
155 for each. The historical development of observational evidence for a direct influence of the QBO
156 on the tropical and subtropical TTL, including radiosonde and zonal mean satellite data, is
157 presented in Section 3. Section 4 shows the seasonal and geographical variation in tropopause
158 temperature, tropopause pressure, and 70-150 hPa zonal wind shear in the 1958-2000 NCEP
159 record for DJF and JJA. Evidence is shown for an amplification of the QBO W-E signal near
160 centers of deep convective center, and effects on the subtropical westerly jet (SWJ). Results for
161 1958-1978 and 1979-2000 are shown separately for comparison.

162 Modern global data sets now include an extra 20 years of observations, increasing the
163 statistical significance of results. Section 5 discusses the distributions of QBO W-E MERRA-2
164 CPT temperature for all four seasons and for the record mean during 1980-2017, in the band
165 20°S-20°N. In section 6, analysis of ERA-Interim data from 1978 – 2018 provides a more
166 complete picture of the QBO signal in the UTLS, including effects on the Walker circulation, the
167 SWJ, seasonal effects in the deep tropics, and a new depiction of the QBO MMC. Section 7
168 summarizes primary findings regarding zonal mean QBO influences, geographical variation, and

seasonal variation in the topics and subtropics, and discusses possible coupling mechanisms that are consistent with the observed geographical variation of enhancement in QBO W-E anomalies.

2. Data and Analysis

2.1. NCEP 1958-2000

In 2001, a range of synoptic charts of QBO W-E differences were created using global reanalysis meteorological fields from NCEP (www.cdc.noaa.gov; Kalnay et al. 1996; Kistler et al. 2001). Monthly averages on a 2.5° grid were calculated from daily averages for the 43-yr period 1958 – 2000 (43 years) and for the two sub-periods 1958 – 1977 (20 years) and 1978-2000 (23 years). Tropopause temperature and tropopause pressure were available as specially-analyzed fields. NCEP tropopause levels were defined with the standard lapse rate definition. Tropical tropopause definitions and seasonal distributions in the tropics are discussed by Hoerling et al. (1991), Tuck et al. (1993), Highwood and Hoskins (1998), Hoinka (1998, 1999), Randel et al. (2000), and Zhou et al. (2001). Seidel et al. (2001) showed that the lapse-rate and CPT definitions yield very similar spatial patterns for climatological tropopause temperature. As will be shown, QBO temperature anomalies in the UTLS exceed 5 km in thickness. The lapse rate tropopause, the CPT, and the 100 hPa surface are less than ~1 km apart vertically in the tropics, which suggests that these minor differences in altitude for analyzing NCEP, MERRA-2, and ERA-Interim data should not strongly impact the resulting patterns of QBO W-E differences.

Prior to 1978, the tropical tropopause was ~3 K cooler than after 1978 in the NCEP record (Pawson and Fiorino 1999, Randel et al. 2000, Huesmann and Hitchman 2003). Due to averaging by phase of the QBO, this discontinuity does not affect results of QBO W-E differences. QBO W-E difference maps were created for 1958-2000 for each season. In order to

192 test for robustness of results, the data were broken into the two periods 1958-1978 and 1979-
193 2000, the results of which are shown in Section 4.

194 Huesmann and Hitchman (2001) explored the relationship between the QBO W-E signal
195 in NCEP tropopause temperature and a QBO index based on the zonal mean zonal wind shear
196 between the paired levels 10-20, 20-30, 30-50, and 50-70 hPa. They found that the 50-70 hPa
197 wind shear index yielded the most coherent QBO W-E signal in the tropical UTLS. Threshold
198 shear values were chosen to be ± 1.5 m s^{-1} $(20\ hPa)^{-1}$ for sorting into QBO W and E categories.
199 Use of a wind shear index provides a clear expectation for the phase of QBO temperature, where
200 westerly shear is vertically coincident with a warm anomaly. This physical expectation allows
201 for the use of a one-tailed Student's t-test. If winds from only one level are used, the location of
202 the thermal anomaly is less certain. While 50-70 hPa shear is highly correlated with 50 hPa
203 wind, the method of determining phase by 50-70 hPa shear was selected to create the NCEP
204 QBO W-E difference maps, which are shown below as Figs. 13-15.

205 During 1958 – 2000 there were ~18 QBO cycles, with 220 westerly, 187 easterly, and
206 109 intermediate months. QBO W-E difference maps were created for each season. Variables
207 examined included tropopause temperature, tropopause pressure, 70-150 hPa wind difference,
208 150 hPa geopotential height, 150 hPa horizontal winds, and 150 hPa relative vorticity. Seasonal
209 means and standard deviations for December-January-February (DJF), March-April-May
210 (MAM), June-July-August (JJA), and September-October-November (SON) were calculated for
211 QBO W and QBO E. Statistical significance was evaluated using a one-sided Student's t-test
212 (assuming that a warm anomaly near the tropical TTL is associated with westerly shear). To
213 evaluate statistical significance, one degree of freedom was assumed for each year (i.e., N = 43
214 for 1958 - 2000, 21 for 1958 -1978, and 22 for 1979 -2000). For a 28-month sinusoidal

oscillation, the autocorrelation as a function of monthly lag decreases from 1.0 to ~ 0.7 in 3.5 months, and becomes negative after 7 months (cf. Fig. 8 of Fraedrich et al. 1993). This suggests that choosing N equal to the number of years in a data record is somewhat too stringent and choosing N equal to the number of months in a data record may be somewhat too lenient. The dependence of the p-value on N for a given t-score is weak, such that an outcome of 95% significance for N=20 increases only to ~96% for N=240. For Figs. 14-16, N was chosen to be the number of years in the record, with light shading indicating confidence levels above 90%, dark shading above 95%, in a 1-tailed Student's t-test.

2.2. MERRA-2 1980-2017

Cold-point tropopause temperatures from MERRA-2 were used for the 38-yr period 1980-2017. Values were interpolated to the CPT using a cubic spline. The phase of the QBO was determined for this analysis using zonal winds at 50 hPa. Zonal wind at 50 hPa is highly correlated with 50-70 hPa zonal wind shear, so the two methods should yield similar results. The range in QBO temperature was defined to be the difference between the warmest and coldest monthly average for each QBO cycle at each location, averaged over all of the cycles during the 38-yr data record (456 total months). Statistical significance was determined by using a two-tailed Students-t test and bootstrapping technique. Each month was assumed to be statistically independent, so that N = 456. Results are shown for QBO range in CPT temperature averaged for the total record and for each season, in the deep tropics (20°S-20°N). In Fig. 17, regions with less than 99% statistical significance are shown in black.

2.3. ERA-Interim 1979-2018

238 The ERA-Interim data assimilation system includes 4-D variational analysis with a 12-hr
239 window (Berrisford et al. 2011, Dee et al. 2011). The resolution of the data set is ~80 km (T255
240 spectral resolution), with 60 pressure levels from the surface to 0.1 hPa. Daily data from the 40-
241 yr period January 1, 1979 – December 31, 2018 were used to create monthly-averaged values of
242 temperature, and the three wind components on pressure surfaces.
243 The phase of the QBO was determined by using the method of Wallace et al. (1993),
244 which projects equatorial zonal wind profiles onto two empirical orthogonal functions (EOFs) in
245 the vertical domain 70 – 10 hPa, to represent the vertical structure for each phase of the QBO.
246 The first two principal components, PC1 and PC2, were defined by EOF analysis based on the
247 covariance matrix of equatorial zonal-mean zonal wind at the five pressure levels 70, 50, 30, 20,
248 and 10 hPa. The annual cycle was first removed by subtracting the 40-yr monthly mean
249 climatology. EOF analysis was performed over the 40-yr ERA-Interim record. When QBO
250 phase is plotted as a function of PC1 and PC2, which vary in time as the QBO descends, the
251 trajectory maps out circles. Eight QBO phases are defined by averaging in 45° angular bins in
252 PC1/PC2 space, where phase-1 is 0°-45°, phase-2 is 45°-90°, phase-3 is 90°-135°, phase-4 is
253 135°-180°, phase-5 is 180°-225°, phase-6 is 225°-270°, phase-7 is 270°-315°, and phase-8 is
254 315°-360°. Phase-4 and phase-8 correspond to when QBO W and QBO E, respectively,
255 maximize in the lower stratosphere. In the current analysis, all the figures are based on Phase-4
256 minus Phase-8. This index corresponds closely to the 50-70 hPa index used for NCEP data and
257 the 50 hPa zonal wind index used for MERRA2 data. Please see Fig. 3 and Section 3 in
258 Wallace et al. (1993) and Fraedrich et al. (1993) for further details.
259 In order to provide a reference frame for the location of QBO anomalies in the UTLS,
260 tropopause pressure was calculated for seasonal means (Fig. 20) and for the record average (Fig.

21). ERA-Interim temperature values were interpolated with a cubic spline to a 1 hPa vertical grid, the traditional lapse rate tropopause pressure was calculated, and then averaged by zonal-mean and by season and data record.

In consideration of possible effects due to the El Nino Southern Oscillation (ENSO), a second data set was generated which only includes ENSO-neutral months (374 months). A neutral ENSO is defined to occur when the sea surface temperature (SST) anomaly from the monthly climatology (40 years) in the Nino3.4 region is between -1.0 K and 1.0 K. The SST data set was obtained from the Hadley Centre Global Sea Ice and Sea Surface Temperature (HadISST) archive. Although results are almost identical for the two data sets, results are shown only for the ENSO-neutral data set.

Statistical significance is calculated by assuming two independent samples, one containing all of the months of phase 4 and another containing all the months for phase 8. The statistical significance test assumes that data for each month is independent from each other, which is the same assumption as made for the MERRA2 data. The number of degrees of freedom assumed was 374. In Figs. 18-21, values which are less than 95% statistically-significant are indicated with diagonal green hatching.

Since seasonal averages are taken, and the QBO has a high autocorrelation for lags of +/- 3 months or less, possible differences of +/- 1-2 months which may result from the three different methods of identifying phase, should not affect results severely. The overall similarity of results from the three analyses suggests that small differences in lag are not important.

3. Observational evidence of a direct influence of the QBO on the UTLS

3.1. 1960-1978: radiosonde analysis and theory of the QBO MMC

In the 1960s progress was made in diagnosing the theoretical structure of the QBO, while observational studies revealed interesting aspects about the QBO, including the degree of downward penetration of QBO wind regimes into the UTLS, the anti-phased relationship between the tropical and subtropical UTLS, and influences on the TTL. Figure 1, from Reed et al. (1961), shows the variation in zonal wind at Canton Island (3°S, 172°W) during the 5 years March 1955 – March 1960. Features of note include the variable periodicity in the range ~22-34 months and variation in shape with altitude. Aspects which contribute to these variations include a more rapid descent rate for QBO westerlies, the existence of time mean easterlies in the middle stratosphere and time mean westerlies in the lower stratosphere, a seasonal modulation of descent rate (e.g., Dunkerton 2017), and seasonal and interannual variability in wave driving.

Note the significant QBO variation in vertical shear of the zonal wind, $\frac{\partial u}{\partial z}$, in the UTLS seen in Fig. 1. This includes the tropical TTL, into which deep convection penetrates to varying degrees (e.g., Folkins et al. 1999, Gettelman and Forster 2002, Gettelman et al. 2002, Dessler et al. 2006, Fueglistaler et al. 2009, Virts et al. 2010; Match and Fueglistaler 2019). Since the tropopause at Canton Island is near 17 km, Fig. 1 suggests that QBO wind regimes mildly influence the tropical upper troposphere. Note also that the sign of 30 hPa zonal wind is often different from the sign of 50-70 hPa wind shear, so it is more useful to use a lower stratospheric QBO index in assessing a "direct effect" on the tropical and subtropical UTLS.

The variation of 50 hPa temperature during 1957-1962 for radiosonde stations at a range of latitudes is shown in Fig. 2 (Angell and Korshover 1964), where the annual cycle has been removed with a 12-month running mean. Note the QBO signal at Canton (3°S), with a temperature range of ~3 K. Note that QBO temperatures in the subtropics tend to be out of phase with the tropics at 50 hPa in the SH during this period. Tucker and Hopwood (1968, their

307 Fig. 3) reported a strong QBO signal and co-variation of zonal wind at Darwin (12°S) and
308 Hobart (43°S) at 28 km altitude for the period 1960-1966. Angell and Korshover (1970, 1974),
309 Wallace (1973), and Newell et al. (1974, Chapter 10) further documented QBO signals in
310 tropical and extratropical lower stratospheric radiosonde temperatures.

311 Theoretical considerations of the QBO by Reed (1966), Wallace (1967), and Dickinson
312 (1968) led to the realization that a zonal mean QBO MMC must exist to maintain the observed
313 relationship between zonal wind and temperature, which is closely approximated by thermal
314 wind balance. Figure 3a shows a schematic diagram of the theoretical QBO structure in
315 temperature and meridional circulation from Dickinson (1968). A warm anomaly centered at the
316 equator should exist below the QBO W maximum, so that $\frac{\partial u}{\partial z} \propto -f \frac{\partial \theta}{\partial y} > 0$, and a cold anomaly
317 should exist below the QBO E maximum, so that $\frac{\partial u}{\partial z} < 0$, to maintain temperature anomalies
318 against radiative relaxation. This requires subsidence below the westerly maximum and ascent
319 below the easterly maximum. This, in turn, implies the existence of a return circulation with
320 opposing vertical motion in the subtropics. The anti-correlation between vertical motion and
321 temperature is expected from a wave-driven circulation. Subsequent versions of this schematic
322 diagram are found in Plumb and Bell (1982), reproduced here as Fig. 3b, and in Gray et al.
323 (1992b), Trepte (1993), and Collimore et al. (2003).

324 Figure 3b reproduces the QBO MMC diagram from Plumb and Bell's (1982) iconic
325 numerical modeling experiments, in which they generated a QBO by parameterized equatorial
326 wave drag in the zonal momentum equation. Their diagram also suggests that the return
327 circulation of the MMC extends outside of the tropics (Fig. 3b). However, observations at the
328 time were as yet insufficient to determine the actual distribution and magnitude of the QBO

329 MMC. A new depiction of the meridional structure of the QBO based on ERA-Interim analyses
330 is shown as a summary diagram at the end of this review (Fig. 21).
331 The extent and similarity of QBO variations in tropopause height throughout Micronesia
332 was described by Reid and Gage (1985). Figure 4 shows that variations in tropopause height
333 with a range of ~200-300 m occurred at time scales of 22-34 months during the period 1952-
334 1982. These stations were all in the deep tropics and QBO variations were in phase.
335 Yasunari (1989) showed that there is an interesting coherence between Singapore zonal
336 winds at 50 hPa and at 700 hPa at QBO periods (Fig. 5), where anomalous westerly flow at 700
337 hPa tends to occur when QBO W are present at 50 hPa. The power in the QBO band at 700 hPa
338 (and at 200 hPa) is ~1/20 that at 50 hPa, so that QBO wind anomalies of 10 m/s at 50 hPa
339 correspond to wind anomalies of perhaps 2 m/s at 700 hPa. Yasunari (1989) showed that QBO
340 wind anomalies at 700 hPa are anti-correlated with 250 hPa winds and argued that the Walker
341 circulation tends to be stronger during QBO E. This would be consistent with strengthened
342 tropical deep convection over Indonesia during QBO E. A study by Knaff (1993) found similar
343 QBO influences on tropical tropospheric winds. It will be shown in Section 6 that analysis of
344 ERA-Interim data supports Yasunari's (1989) idea that the Walker circulation tends to be weaker
345 during QBO W.
346
347 *3.2. 1978-1994: Satellite observations of stratospheric temperature and aerosol*
348 The launch of limb-scanning instruments on board polar-orbiting satellites in the late
349 1970s afforded an unprecedented view of stratospheric temperature and volcanic aerosol,
350 including the limb infrared monitor of the stratosphere (LIMS) instrument (Gille and Russell
351 1984), which measured temperature, the Stratospheric Aerosol and Gas Experiment (SAGE I and

352 II) instruments (McCormick et at. 1989), which sampled aerosol in the tropics and midlatitudes,
353 and the Stratospheric Aerosol Measurement (SAM II) instrument (Russell et al. 1981), which
354 observed aerosol in the polar regions.

355 In diagnosing the distribution of zonal mean temperature, zonal wind, and absolute
356 vorticity in LIMS data, Hitchman and Leovy (1986) argued that the QBO MMC modulates the
357 distribution of temperature and absolute vorticity. Figure 6 shows zonal mean sections of these
358 variables, for the period October 31 – November 5, 1978, when QBO W were in the lowest
359 stratosphere and QBO E were centered near 10 hPa (Fig. 6b). In Fig. 6c, normalized absolute
360 vorticity is plotted: $\frac{f}{|f|}\left(f-\frac{\partial \overline{u}}{\partial y}\right)$, such that negative regions indicate anomalous absolute vorticity
361 for the given hemisphere. The zero-wind line near 10 hPa separates QBO E below from QBO W
362 above (Fig. 6b). Near 10 hPa, the temperature contours are pinched together over the equator
363 and spread out vertically in the subtropics, consistent with the MMC indicated by the arrows in
364 Fig. 6a. The distribution of absolute vorticity in Fig. 6c is also consistent with redistribution by
365 the QBO MMC, where contours are spread apart just above the level of the QBO E wind
366 maximum at ~10 hPa, with enhanced gradients in the subtropics near 25°S and 25°N. Near 50
367 hPa, contours appear pinched together towards the equator by a convergent flow (Fig. 6c). These
368 results support the idea that the QBO MMC can affect the extratropics.

369 Trepte and Hitchman (1992) and Hitchman et al. (1994) used SAGE I and II and SAM II
370 aerosol data to study the structure of the QBO. Fall velocities for ~0.1-1 μm diameter droplets of
371 aerosol in the lower stratosphere are on the order of 0.1-0.5 mm/s. Since this is comparable to
372 theoretical estimates of the magnitude of vertical motion associated with the QBO MMC, the
373 distribution of volcanic aerosol can act as a "dye" to reveal the structure of the QBO MMC.
374 Trepte and Hitchman (1992) showed sample 40-day "snapshots" of aerosol distributions in

latitude-altitude which highlighted the QBO MMC. During QBO W (Fig. 7a) characteristic "horns" may be seen above the W maximum, compatible with sinking over the equator and rising motion in the subtropics. During QBO E (Fig. 7b), air is gathered and lofted over the equator, creating a narrower, taller vault of high aerosol concentrations.

Hitchman et al. (1994) showed that the QBO modulates the tropical aerosol reservoir, such that, during QBO W, optical depth is reduced in the tropics and enhanced in the subtropics. Figure 8 shows QBO W-E difference in aerosol extinction ratio values based on 10 years of data, with differences on the order of 20-50%. During QBO W, descent occurs over the equator, with enhanced poleward motion and rising in the subtropics, spreading volcanic aerosol from the "tropical reservoir" into the extratropical lower stratosphere in a "lower transport regime" (Hitchman et al. 1994). During QBO E, aerosol is gathered and lofted in the tropical reservoir. Choi et al. (2002) analyzed the QBO influence on trace constituents from the Halogen Occultation Experiment (HALOE). They also found and a strong modulation of tracer distributions by the QBO MMC.

Figure 9 shows a schematic diagram of the effects of the QBO MMC on temperature and tropopause altitude, taken from Collimore et al. (2003). It is similar to figures in Gray et al. (1992b) and Trepte (1993). During QBO W (Fig. 9a), absorption of waves with westerly phase speeds causes westerly acceleration and convergent, equatorward flow, which imports lower angular momentum air from higher latitudes (Lindzen and Holton 1968). Mass convergence implies subsidence warming in the tropics and cooling by ascent in the flanking subtropics, with the resulting temperature anomalies yielding a consequent displacement of the tropopause downward in the tropics and upward in the subtropics. During QBO E (Fig. 9b), easterly wave drag causes easterly acceleration and poleward divergence. This requires ascent in the tropics

and descent in the subtropics, with an upward deformation of the tropopause in the tropics and downward in the subtropics. A new climatology of the QBO MMC will be shown in Figs. 20 and 21.

In addition to QBO effects on the UTLS, other studies have found relationships between the QBO and tropical weather phenomena. Angell et al. (1969) suggested that Atlantic hurricanes are more plentiful during QBO W. Gray (1984) and Gray et al. (1992b) also found that the QBO influences Atlantic hurricane frequency, with QBO W favoring more hurricanes. They suggested that stronger westerly shear in the subtropical North Atlantic UTLS associated with QBO W reduces the local climatological easterly wind shear across the UTLS, thereby fostering growth of tropical cyclones. Gray and Schaeffer (1991) found evidence for QBO modulation of tropical cyclones in other ocean basins. Ho et al. (2009) showed that the QBO modulates the preferred longitude band of tropical cyclones in the western Pacific. However, Camargo and Sobel (2010) showed that the correlation between tropical cyclones and the QBO depends on the period of observation. Further observational study over a longer time may be required to understand this problem.

QBO effects on tropical rainfall have been reported by Hastenrath (1990), Gray et al. (1992a), and Kane (1995). In a study of outgoing longwave radiation (OLR) over Indonesia, Knaff (1993) showed that deep convection tends to be stronger, as seen in reduced OLR emitted from colder cloud tops, when QBO E shear is in the tropical UTLS. Collimore et al. (1998) showed that QBO E in the lower stratosphere favors more extensive deep convection in the three primary centers of chronic convection, Amazonia, Africa, and Indonesia, with effects being most notable during boreal winter.

3.3. 1994-2000: QBO effect on the zonal mean TTL in global analyses

The first attempt to make a quantitative estimate of the latitudinal structure of the QBO in temperature in the lower stratosphere was made by Reid (1994), who calculated temperature anomalies, based on observed QBO variations in zonal wind, from the thermal wind law applied in the vicinity of the equator:

$$\frac{\partial T}{\partial y} = -\frac{2\,\Omega\,T\,y}{g\,R}\,\frac{\partial u}{\partial z} \qquad (1)$$

where u, T, and y are zonal wind, temperature, and latitude in meters, while Ω, g and R are the earth's rotational angular velocity, gravitational acceleration, and radius. Assuming a typical value for shear of 3 m/s per 6 km and a mean equatorial temperature of 210 K, he estimated that, during QBO W, temperatures would be ~3 K warmer over the equator and ~3 K cooler near 30°S and 30°N compared to during QBO E (Fig. 10). This estimated range of 3 K turns out to be somewhat higher than in the results shown in Sections 4-6.

Randel et al. (1999) used stratospheric analyses from the United Kingdom Meteorological Service (UKMO) to estimate vertical velocities associated with the QBO MMC, by assuming that vertical advection balances radiative heating/cooling associated with a QBO temperature anomaly. They found upward motion in cold anomalies, with estimated QBO vertical motion magnitudes of less than 0.1 mm/s below 30 hPa (cf. their Fig. 13).

Randel et al. (2000) investigated interannual variability of the tropical tropopause derived from radiosonde data and NCEP reanalyses. They found "a strong signature of the QBO in tropopause statistics" that is primarily zonal mean in character. Using regression analysis on zonal winds for the period 1979-1997, they estimated the latitudinal variation of tropopause temperature and tropopause pressure associated with the QBO (Fig. 11). They confirmed the anti-phased nature of the signal in the tropics and subtropics and estimated a range of ~1 K in

444 tropical tropopause temperature and ~2 hPa in tropical tropopause pressure, assuming a range of
445 40 m/s for the QBO in zonal wind.

446 Huesmann and Hitchman (2001) analyzed QBO variations in NCEP tropopause
447 temperature, tropopause pressure, and zonal winds in the UTLS for the period 1978-2000.
448 Figure 12a shows the zonal mean distribution of tropopause temperature for DJF. Figure 12b
449 shows latitudinal profiles of QBO W and E anomalies. This shows a QBO range in zonal mean
450 tropical tropopause temperature of ~1 K, with smaller, anti-phased maxima centered near 30°S
451 and 30°N and extending into the extratropics.

452 In contrast, NCEP 50-70 hPa zonal wind QBO zonal wind shear anomalies are of
453 uniform sign for a given QBO wind regime across the range ~25°S – 25°N, but are negligible
454 outside of the tropics for this layer (Fig. 13). This is useful to keep in mind for interpreting
455 seasonal synoptic charts of 70-150 hPa zonal wind shear in Section 4. The QBO range in 50-70
456 hPa wind shear is ~10 m/s per 20 hPa.

457

458 **4. 2001: NCEP seasonal and geographical variation of QBO signal in the UTLS**

459 *4.1. NCEP tropopause temperature*

460 The geographical distribution of seasonal mean and QBO W-E differences in NCEP
461 tropopause temperature are shown for DJF and JJA in Fig. 14. Coldest temperatures during DJF
462 occur over Amazonia, Central Africa, and the West Pacific warm pool, with temperatures less
463 than 192 K over the Amazon and Western Pacific (Figs. 14e, f). These are the locations of
464 chronic deep convection, characterized by low OLR and high rainfall rate (e.g., Collimore et al.
465 1998). During JJA, the Western Pacific deep convection shifts toward India, and Amazonian
466 convection shifts toward the Gulf of Panama. Tropopause temperatures are 2-4 K warmer

467 throughout the tropics during JJA, and there is less geographical variation compared to DJF
468 (Figs. 14g, h). Slight variations in the pattern and magnitude of tropopause temperature are seen
469 between 1958-1978 and 1979-2000 (compare Figs. 14e and f, g and h). These seasonal-mean
470 distributions agree well with those of Seidel et al. (2001, Fig. 11), who used radiosondes from
471 1961-1990, Highwood and Hoskins (1998, Fig. 6), who used ECMWF data from 1991-1995, and
472 Hoinka (1999, Fig. 2), who used ECMWF data from 1979-1993.

473 Distributions of QBO W-E differences in tropopause temperature are shown for DJF and
474 JJA in Figs. 14a-d. During QBO W, tropical tropopause temperatures are warmer, and
475 subtropical temperatures are generally colder, in agreement with the zonal mean results shown in
476 Figs. 10-13 and with theoretical expectations from the QBO MMC. Statistical significance is
477 fairly high throughout the tropics, where the range reaches 1.5 K, and is somewhat smaller
478 during JJA and during the second half of the data record. Another statistically-significant zonal
479 mean QBO signal is seen near 25°S during JJA, with range reaching 1.5 K (Figs. 14c, d). In this
480 case, the signal is larger during the second half of the data record. This pattern is reminiscent of
481 the latitudinal anti-phasing in the SH found by Angell and Korshover (1964) (Fig. 2).

482 Assuming that enhanced tropical upwelling is related to a cooler TTL, this zonal mean
483 QBO signal is compatible with a reduction of the Brewer-Dobson circulation during QBO W. It
484 is consistent with the results of Eluskiewicz et al. (1996) and Yang and Tung (1996), who found
485 that the global circulation in the lower stratosphere is weaker during QBO W, and with Seol and
486 Yamazaki (1998), who showed that the upward mass flux across 100 hPa in the tropics is
487 reduced during QBO W.

488 In addition to the zonal mean QBO signal, significant geographical variations, or zonal
489 asymmetries, occur. These zonal asymmetries appear to be linked to the distribution of

490 continents and seasonal monsoon structures. During DJF, the temperature range is largest in a
491 band extending from South America, increasing eastward to ~1.6 K near Indonesia (Figs. 14a,
492 b). The location of the maximum near Indonesia during DJF differs somewhat during the two
493 periods (Figs. 14a, b). The maximum found in the eastern Pacific during 1958-1978 (Fig. 14a) is
494 largely absent during 1979-2000 (Fig. 14b). During JJA (Figs. 14c, d), QBO W-E differences
495 maximize over the Atlantic, Indian, and Pacific Oceans.
496 Zhou et al. (2001) interpolated global ECMWF data at standard pressure levels for the
497 period 1979 – 1993 to estimate CPT levels. Daily values were then sorted by QBO phase
498 according to a 40 – 70 hPa shear index, with lag 6 months. Their Fig. 7 shows the annual mean
499 distributions of CPT temperatures for QBO W and QBO E in the latitude band 25°S-25°N.
500 Differences of ~0.4-0.8 K occur, with a maximum in the Eastern Pacific.
501 Collimore et al. (2003) described QBO W-E differences for OLR and highly reflective
502 cloud (HRC) for each season, which showed reduced deep tropical clouds during QBO W. They
503 also showed QBO W-E differences in tropopause temperature for each season, using NCEP data
504 from the 17-yr period 1971-1987 and using the 50 – 70 hPa shear index with no lag. They
505 confined their presentation to the band 25°S-25°N, which excludes the anti-phased subtropical
506 features. Similar to the results of Zhou et al. (2001), their QBO range in the tropics showed a
507 maximum in the Eastern Pacific. The sparseness of radiosonde observations in the Eastern
508 Pacific renders a signal less reliable in this region. Anstey et al. (2020) suggested that, over
509 time, better analysis methods and satellite temperature data have helped to ameliorate this
510 problem. The seasonal and geographical dependence of the QBO signal in MERRA-2 CPT
511 temperature and ERA-Interim data is explored in detail in Sections 5 and 6.
512

513 *4.2. NCEP tropopause pressure*

514 Climatological tropopause pressure and QBO W-E differences in tropopause pressure are
515 shown for DJF and JJA in Fig. 15. Tropopause pressures are less than 100 hPa throughout most
516 of the tropics during DJF (Figs. 15e, f) and near India during JJA (Figs. 15g, h). These seasonal
517 mean tropopause pressure distributions agree well with Hoinka (1998, Fig. 2) and Seidel et al.
518 (2001, Fig. 9).

519 Tropopause pressures are higher throughout the tropics during QBO W than during QBO
520 E (Figs. 15a-d). This is compatible with the zonal mean results of Randel et al. (2000), shown in
521 Fig. 11b, and with Fig. 3c of Collimore et al. (2003). As with tropopause temperature (Figs. 14a-
522 d), differences in the tropics are larger and more statistically significant during DJF than in JJA,
523 and during the first half of the data record. Again, significant zonal asymmetries are evident.
524 QBO differences in tropopause pressure are larger over the Western Pacific during DJF (Figs.
525 15a, b) and over each of the three oceans during JJA (Figs. 15c, d). The QBO range in
526 tropopause pressure exceeds ~3 hPa near Indonesia during DJF (Figs. 15a, b).

527 As with tropopause temperature, there is an interesting hemispheric asymmetry, with an
528 amplified, statistically-significant QBO signal in tropopause pressure near 25°S during JJA
529 (Figs. 15c, d). This is especially notable during the second half of the data record, with range
530 exceeding ~6 hPa (Fig. 15d).

531 To relate changes in tropopause pressure to changes in tropopause altitude one may use
532 the hydrostatic equation $\delta p = -\rho\, g\, \delta z$. Assuming $\rho \sim 0.1$ kg m^{-3} near the tropopause, an
533 increase of 100 Pa (1 hPa) in tropopause pressure corresponds to a 100 m decrease in tropopause
534 altitude. From Fig. 15, one might expect the tropical tropopause during QBO W to be ~100-300

535 m lower than average in DJF and ~100 m lower in JJA. This is compatible with the results of
536 Reid and Gage (1985) shown in Fig. 4.
537
538 *4.3. NCEP 70 – 150 hPa wind shear*
539 The DJF and JJA average distributions of 70 – 150 hPa zonal wind shear are shown in
540 Figs. 16e-h. This layer spans the depth of the TTL, as defined by Fueglistaler et al. (2009).
541 Westerly shear is found over Amazonia and over a broad region extending from Africa to
542 Indonesia, reaching 15 m/s per 80 hPa over Indonesia during DJF (Figs. 16e, f). This pattern is
543 shifted slightly westward during JJA, reaching 25 m/s per 80 hPa over the Indian Ocean (Figs.
544 16g, h). During JJA, westerly shear is enhanced in the eastern hemisphere by the upper
545 tropospheric easterlies which lie equatorward of the Tibetan High. Since seasonal mean winds
546 are weak near 70 hPa, geographical and seasonal variations in 70 – 150 hPa shear are primarily
547 due to variations at 150 hPa. The region of westerly shear over the Amazon is more robust in
548 the second half of the data record (compare Fig. 14e with 14f, and 14g with 14h).
549 In the extratropics, 70-150 hPa wind shears are generally negative (Figs. 16e-h). The
550 easterly shear and zonal variation in this pattern near $\pm 30°$ is due the presence of the SWJ,
551 which varies in longitude and season. Strong easterly shear is found above the SWJ near 30°N
552 during DJF, reaching -35 m/s per 80 hPa over Japan (Figs. 16e, f), and near 30°S over Australia
553 during JJA (Figs. 16g, h).
554 QBO W-E differences in 70-150 hPa zonal wind shear for DJF and JJA are shown in
555 Figs. 16a-d. The sign of the shear is retained so that one might visually add the QBO W- E
556 perturbation to the seasonal average field and determine whether UTLS wind shear is diminished
557 or enhanced locally by the QBO. During QBO W, 150-70 hPa wind shears are more westerly by

558 3-8 m s^{-1} per 80 hPa throughout most of the tropics (Figs. 16a-d), in agreement with the zonal
559 mean results in Fig. 13b. QBO differences in 70-150 hPa wind shear are generally statistically
560 significant throughout the tropics. During DJF, maxima are found over Amazonia, Africa, and
561 Indonesia (Figs. 16a, b), where the basic state shear is westerly (Figs. 16e, f). During JJA, a
562 maximum is found extending from South America eastward to Indonesia (Figs. 16c, d). A
563 notable difference is found between the two periods near New Guinea, where the QBO signal is
564 larger during 1979-2000 (Figs. 16c, d).
565 The basic state 70-150 hPa wind shear over the subtropical North Atlantic during JJA is ~
566 -10 to -15 m/s per 80 hPa (Figs. 16g, h). During QBO W, the predominant seasonal mean
567 easterly shear in the subtropical North Atlantic would be diminished by ~1-3 m/s per 80 hPa
568 (Figs. 16c, d, g, h). This type of information can be useful in considering Gray et al.'s (1992a)
569 hypothesis that tropical deep convection, including tropical cyclones, might be more robust in
570 reduced UTLS wind shear.
571 Considering the tropics, QBO E would act to diminish the westerly shear seen over
572 centers of deep convection over Amazonia and from Africa to Indonesia (Figs. 16e-h). If Gray et
573 al.'s hypothesis is correct, this would suggest that tropical deep convection would be enhanced in
574 these regions during QBO E.
575 QBO W-E differences in 70 – 150 hPa shear exhibit a node near 25° latitude, with shears
576 tending to be more easterly during QBO W near 30° latitude (Figs. 16a-d). Figure 13b shows
577 that QBO differences in 50 – 70 hPa wind shear are negligible poleward of ~25° latitude. This
578 suggests that the difference occurs at 150 hPa, with QBO W favoring stronger SWJs (which
579 would make 70 - 150 hPa shears more easterly). The strength and seasonality of the observed
580 QBO influence on the SWJs is re-examined using ERA-Interim data in Section 6.

581 The QBO signal in the tropical UTLS is less robust during 1978-2000 than during 1958-
582 1978 in the NCEP record. This was previously shown in Figs. 13a and 14 of Randel et al.
583 (2000). Recent comparisons of the zonal mean QBO signal in a range of global analyses also
584 show that the NCEP signal during 1978-2000 is somewhat weaker than in other analyses
585 (Tegtmeier et al. 2020; Martin et al. 2020).
586 The geographical variation of the QBO signal and its seasonal dependence as seen in
587 NCEP data during 1958-1978 and 1979-2000 are now compared with two modern global
588 reanalysis data sets. We first explore the seasonal QBO signal in tropopause temperature in
589 MERRA-2 data for 1980-2017, focusing on the QBO range in CPT temperature in the deep
590 tropics. This is followed by an analysis of results from ERA-Interim data in the domain 40°S-
591 40°N, 1000-1 hPa, for the period 1979-2018.
592
593 **5. QBO W-E MERRA-2 CPT temperature**
594 Figure 17 shows the annual and seasonal mean distributions of the range in QBO W-E
595 CPT temperatures in MERRA-2 analyses for the 38 years 1980-2017, in the domain 20°S-20°N.
596 In the annual mean (Fig. 17a), one may observe a broad equatorial maximum, with values
597 reaching ~2 K near the west coast of South America, over Africa, and Indonesia. A node, or
598 minimum in QBO range, is seen in MERRA-2 CPT temperature near ~15° latitude, where
599 statistical significance can fall below 99%. This is similar to the average latitude of the zero-
600 line for QBO W-E tropopause temperature seen in Figs. 14a-d.
601 The QBO W-E range in MERRA-2 CPT temperature varies considerably with season,
602 with larger values during DJF and MAM (Fig. 17b, c), contributing fundamentally to the
603 geographical pattern seen in the annual average (Fig. 17a). During DJF, maxima are observed

604 over the west coast of South America and stretching from Africa to Indonesia, with a secondary
605 maximum over the Western Pacific (Fig. 17b). This zonally asymmetric pattern for DJF seen in
606 MERRA-2 data is similar to what was found for the NCEP data (Figs. 14a, b), but with
607 maximum amplitudes over Indonesia of ~2.2 K instead of ~1.8 K.

608 During MAM, the pattern is similar to DJF, but with a reduction in the Western Pacific
609 and enhancement in the Eastern Pacific (compare Figs. 17b, c). Amplitudes during MAM are
610 larger than during DJF near South America, and extending from Africa to Indonesia, reaching
611 2.5 K. It may be relevant that in March the coldest climatological temperatures occur over
612 Africa (Tuck et al. 1993).

613 During JJA and SON, the QBO range in CPT is less than ~1.4 K. During JJA, a
614 maximum occurs over the Atlantic/African sector, with a secondary maximum over Indonesia
615 (Fig. 17d). This is in broad agreement with results from NCEP data (Figs. 14c, d). During
616 SON, the pattern is similar to JJA in the Atlantic/African sector (Fig. 17e), but two other maxima
617 occur over the west coast of South America and Western Pacific (Fig. 17e).

618

619 **6. Analysis of ERA-Interim data during 1979-2018**

620 *6.1. ERA-Interim 100 hPa temperature*

621 The geographical distributions of QBO W-E (phase-4 minus phase-8) differences for 100
622 hPa temperature in ERA-Interim data during 1979 – 2018 are shown for each season in Fig. 18.
623 In agreement with results for NCEP and MERRA-2 tropopause temperatures, QBO differences
624 in 100 hPa temperature have a significant zonal mean component, with a typical range of 1-2 K,
625 and QBO W favoring higher 100 hPa temperatures in the tropics and lower temperatures in the
626 subtropics.

627 Significant geographical variations are also evident. During DJF (Fig. 18a), QBO W-E
628 differences are larger over Amazonia, Africa and Indonesia, in a pattern similar to Figs. 14a, b
629 and 17b. The range reaches 1.5 K over Indonesia during DJF in the ERA-Interim data (Fig.
630 18a).
631 During MAM (Fig. 18b), the statistically significant region in the tropics is much larger,
632 extending from the far Eastern Pacific eastward to the Date Line, with largest ranges (1.5 K) over
633 Amazonia, Africa, and Indonesia. Also of significance during MAM are the pronounced QBO
634 W cold regions near 25°S and 25°N during QBO W, to be further discussed in Section 6.4.
635 During JJA (Fig. 18c), a QBO W-E range maximum extends from Brazil to East Africa,
636 reaching 1.2 K, with a second maximum in the Eastern Indian Ocean. This is in agreement with
637 Figs. 14c, d and Fig. 17d. Note also the statistically significant negative region near 25°S during
638 JJA (Fig. 18c), in agreement with results shown in Fig. 14d. During SON (Fig. 18d), tropical
639 QBO differences are similar to in JJA, but with another maximum over the Eastern Pacific, in
640 agreement with Fig. 17e. There is also evidence of a moderate QBO signal near 25°S and 25°N
641 during SON (Fig. 18d), similar to that seen during MAM (Fig. 18c).
642 A detailed inspection of the QBO W-E signal in MERRA-2 CPT temperature (Fig. 17)
643 and ERA-Interim 100 hPa temperature (Fig. 18), for each season, shows that they are remarkably
644 similar in distribution and magnitude. These modern data sets confirm many of the features seen
645 in the NCEP analysis, including a tendency for maxima to occur near centers of deep convection,
646 and a large QBO range near 25°S during JJA. The anti-phased response in the subtropics is
647 most pronounced in the SH during JJA, and in both hemispheres during MAM and SON.
648
649 *6.2. ERA-Interim 150 hPa zonal wind*

650 The geographical distributions of seasonal means and QBO W-E differences in 150 hPa
651 zonal wind are shown in Fig. 19. The 150 hPa level lies below the tropical tropopause, extends
652 through the center of the SWJs near 30°S and 30°N, and into the extratropical lower stratosphere.
653 During DJF, easterly flow is seen over Amazonia, Africa, and Indonesia, near regions of deep
654 convection (Fig. 19e). Elsewhere, westerlies are observed, reaching maxima in the SWJs near
655 30°S and 30°N. During MAM, the pattern of easterlies is similar to DJF, but with reduced
656 strength in the eastern hemisphere, and light westerlies over Amazonia (Fig. 19f). During JJA,
657 the region of easterlies greatly expands and strengthens, extending from the Western Pacific
658 westward to Brazil (Fig. 19g). This is consistent with the development of the Tibetan High
659 during NH summer. Note also the center of easterlies over the far Eastern tropical Pacific, near
660 the region of deep convection in the Gulf of Panama (Fig. 19g). During SON, the pattern is
661 similar to JJA but somewhat reduced in amplitude and extent (Fig. 19h).
662 Seasonal mean patterns of NCEP 70-150 hPa zonal wind shear (for the period 1978-
663 2000) and ERA-Interim 150 zonal wind show good agreement between regions of westerly 70-
664 150 shear and regions of 150 hPa easterlies for both DJF and JJA (compare Figs. 16e, f with 19e,
665 and 16g, h with 19g). This lack of westerly shear over the far Eastern tropical Pacific in the
666 1958-1978 NCEP data (Figs. 16e, g) suggests that satellite data have since improved the
667 accuracy of this feature.
668 During QBO W, the SWJs tend to be stronger in each season, with ranges of 1-7 m/s, but
669 with variable statistical significance (Figs. 19a-d). During DJF (Fig. 19a), statistically significant
670 differences are seen over the Caribbean, North Africa, and India in the NH, and over Australia
671 and the mid-Pacific in the SH. Also of interest during DJF is the easterly anomaly over the
672 tropical Atlantic for QBO W.

673 During MAM (Fig. 19b), the signal in both subtropics is more robust than during DJF,
674 with centers of significant westerly enhancement of the SWJ over North Africa and from East
675 Asia eastward to the Atlantic in the NH. Note the large easterly anomaly over the eastern
676 tropical Pacific in the upper troposphere during QBO W in MAM (Fig. 19b). This is consistent
677 with a reduced Walker circulation during QBO W, and tends to confirm Yasunari's (1989)
678 suggestion that the QBO can modulate the Walker circulation.
679 During JJA (Fig 19c), the QBO signal in 150 hPa winds is generally weaker, except for a
680 strong signal in the SH subtropics. During SON (Fig. 19d), the signal is similar to JJA, but
681 weaker in the SH subtropics and stronger in the NH subtropics.
682 Wang et al. (2017), in an investigation of the QBO effect on NH storm tracks, showed
683 meridional sections of zonal wind together with QBO W and QBO E anomalies, averaged for the
684 Pacific and Atlantic sectors. They used ERA-Interim data averaged for October – March,
685 during the period 1979 - 2016. Their Fig. 1 shows that QBO W strengthens the SWJ in both the
686 Atlantic and Pacific sectors, but QBO E favors a poleward displacement in the Pacific sector.
687 These results are consistent with Fig. 19a, and with the numerical modeling results of Garfinkel
688 and Hartmann (2007, 2011).
689 In summary, QBO W-E differences for ERA-Interim 150 hPa zonal winds tend to show
690 an enhancement of the SWJs during QBO W. As with 100 hPa temperature, the response in the
691 subtropics is most pronounced during MAM in both hemispheres and during JJA in the SH, with
692 moderate signals during DJF in the NH and during SON in both hemispheres. More can be
693 understood about this relationship by examining variation in the meridional plane throughout the
694 UTLS.
695

696 *6.3. ERA-Interim seasonal structure of QBO anomalies in meridional plane*

697 Seasonal mean distributions of QBO W-E zonal mean anomalies of ERA-Interim zonal
698 wind and temperature, with superimposed vectors of the MMC are shown in Fig. 20, for the
699 domain 40°S-40°N, 1000 – 1 hPa. Each seasonal mean tropopause is also indicated. This
700 depiction of phase-4 minus phase-8 selects for a positive westerly wind anomaly near 50 hPa
701 (~21 km) over the equator, with an easterly maximum near 10 hPa (~30 km) and another
702 westerly maximum near 2 hPa (~58 km), giving a vertical wavelength of ~27 km, as seen in each
703 season (Figs. 20a-d).

704 The tropical westerly wind anomaly near 50 hPa exhibits an interesting poleward and
705 downward extension into the subtropical UTLS near the SWJs. This effect is most noticeable in
706 the SH during JJA (Fig. 20c) and during MAM in both hemispheres (Fig. 20b). More moderate
707 effects are also seen in both hemispheres during DJF (Fig. 20a) and in the SH during SON (Fig.
708 20d). This signal in the zonal mean confirms QBO W-E features diagnosed in 150 hPa zonal
709 wind (Fig. 19), and provides a broader context for the 150 hPa signal in terms of the QBO MMC.

710 During QBO W there is an extensive and statistically significant easterly zonal wind
711 anomaly in the tropical upper troposphere, but only during DJF and MAM (Fig. 20a, b). During
712 MAM, this negative anomaly reaches 3 m/s (Figs. 20b). This signal is a zonal average of the
713 large negative anomaly in Figs. 19a, b, which reaches 9 m/s in the eastern tropical Pacific in
714 MAM (Fig. 19b). The negative region spans the upper troposphere in the tropical eastern
715 Pacific, the eastward half of the Walker circulation. QBO W reduce the Walker circulation,
716 especially during MAM. During MAM, there are also statistically-significant warm temperature
717 anomalies in the upper troposphere near 20°S and 20°N during QBO W (Fig. 20f), which are
718 related to strengthening of the SWJ (Fig. 20d) through thermal wind balance. This has

719 implications for the "East Pacific Tropical Rossby waveguide", where westerly winds associated
720 with the Walker circulation allow Rossby wave energy to travel between hemispheres (Webster
721 and Holton 1982). During MAM, this would be less likely to occur during QBO W.
722 QBO W-E equatorial positive temperature maxima occur near 70 hPa and 5 hPa, with a
723 cold anomaly near 30 hPa (Figs. 20e-h). During the equinoxes (Figs. 20f, h), the temperature
724 anomaly pattern is equatorially symmetric, in a 9-element "checkerboard" pattern centered on
725 the tropical cold anomaly near 30 hPa, with stacked cells of the opposite sign maximizing near
726 30°S and 30°N and extending into midlatitudes.
727 During the solstices this pattern is warped, such that larger warm anomalies are found on
728 the winter side near 30 hPa (Figs. 20e, g), which suggests that the QBO MMC is stronger in the
729 winter subtropics. The MMC is also stronger on the winter side. This may be related to
730 enhanced planetary wave drag in the subtropical winter hemisphere. This seasonal modulation
731 of the QBO has been discussed by Randel et al. (1999), Kinnersley (1999), and Pena-Ortiz et al.
732 (2008).
733 QBO W-E vertical motion anomalies are anti-correlated with the temperature anomalies
734 due to adiabatic cooling/heating. This relationship is expected from a wave-driven circulation,
735 where upward motion advects low potential temperature air upward, creating a cold anomaly.
736 This "checkerboard" pattern of vertical motion comprises three stacked MMCs of alternating
737 sign in the subtropics. These seasonal climatological meridional distributions provide an
738 integrative view of QBO W-E anomalies of wind and temperature at different locations and
739 latitudes, including the anti-phased relationship between the tropical and subtropical TTL.
740
741 *6.4. ERA-Interim time mean QBO anomalies of zonal wind, temperature, and MMC*

742 The time mean distribution of QBO W-E ERA-Interim zonal mean zonal wind,
743 temperature, and MMC is shown in Fig. 21. The QBO range in zonal wind at the equator near
744 50 hPa is ~25 m/s (Fig. 21a). The QBO range in temperature at the equator near 70 hPa is ~2 K,
745 with the warm anomaly extending below the tropopause (Fig. 21b). In the tropical upper
746 troposphere, there is a statistically QBO signal with range exceeding 2 m/s, extending into the
747 middle troposphere (Fig. 21b). This annual mean preserves some of the strong signal seen in
748 MAM in Fig. 20b, which is largely due to a reduced eastward flow in the Eastern Pacific (Fig.
749 19c). Enhancement of the SWJs by ~2 m/s during QBO W is seen in Fig. 21a, with a
750 statistically-significant region extending downward into the troposphere. Statistical significance
751 is higher for the QBO signal near the SWJs relative to Fig. 19, due to zonal and time averaging.
752 The time-mean QBO W-E temperature anomaly pattern (Fig. 21b) shows a
753 "checkerboard" grid with a statistically significant warm anomaly during QBO W in the upper
754 troposphere, consistent with reduced upwelling in the tropics. The time-mean QBO W-E vertical
755 velocity anomaly pattern is the same as, but opposite in sign to, the temperature anomaly pattern
756 (Fig. 21b). Note the statistically-significant negative vertical velocity anomaly in the tropical
757 upper troposphere and statistically-significant positive anomalies near 100 hPa at 20°S and 20°N.
758 This is compatible with a reduced Brewer-Dobson circulation in the lowest stratosphere during
759 QBO W. A more complete description of this QBO temperature pattern is that a warm QBO
760 anomaly in the TTL is accompanied by a cold anomaly which extends continuously poleward
761 and downward all the way into the midlatitudes in the UTLS (note downward-sloping cold
762 maxima along the tropopause in Fig. 21b). By including all seasons, greater statistical
763 significance is achieved, confirming the influence of the QBO on the SWJ, Hadley cell, and
764 Walker circulation.

765

766 **7. Summary of observational studies and discussion of mechanisms**

767 *7.1. Summary of observational results*

768 Studies of radiosonde observations in the 1960s showed that the influence of the QBO
769 extends downward into the tropical upper troposphere, modulating the altitude of the tropopause,
770 and that anti-phased temperature anomalies occur in the tropical and subtropical TTL.
771 Simultaneously, theoretical development showed that the QBO requires an MMC, the result of
772 being wave-driven, and that this circulation spatially integrates features in altitude and latitude.
773 The existence of a QBO MMC was confirmed in satellite-derived distributions of temperature
774 and aerosol. Several authors suggested that the QBO might have other effects on tropical
775 weather, including modulation of the Walker circulation, precipitation, and tropical cyclones.
776 These studies raised the possibility that the QBO might somehow modulate tropical deep
777 convection.

778 The advent of satellite data and global analyses allowed confirmation of the zonal mean
779 QBO signal for tropopause temperature and pressure, with anti-phased anomalies in the tropics
780 and subtropics. During QBO W in the lower stratosphere, the tropical tropopause is lower and
781 warmer, with stronger westerly wind shear in the tropics, stronger SWJs, and a weaker Walker
782 circulation. During QBO E in the lower stratosphere, the tropical tropopause is higher and
783 colder, with enhanced easterly wind shear in the tropics and a stronger Walker circulation.
784 Seasonal maps of NCEP QBO W-E differences in tropopause temperature and pressure showed
785 that the subtropical anomaly is largest in the winter hemisphere. They also showed that the QBO
786 range in tropopause temperature exhibits significant geographical variation, with largest values
787 over centers of deep tropical convection, most notably over Amazonia, Africa, and Indonesia

788 during DJF and over the Atlantic and Indian Oceans during JJA. These results suggest that there
789 is some form of coupling between the QBO and tropical deep convection.

790 A modern update and extension of this analysis was shown using 38 years of MERRA-2
791 CPT data in the deep tropics, and 40 years of ERA-Interim data from 1979 – 2018, where
792 months with a significant ENSO signal were removed from the record. Keeping in mind that the
793 tropopause is not the same as the 100 hPa surface, that the QBO sorting algorithms were slightly
794 different, and that the time periods were different, the salient features from the NCEP study were
795 confirmed, including seasonal and geographical variation of the QBO temperature response, and
796 a strong signal in the SH winter subtropics. Improved statistical significance and data reliability
797 provides greater confidence in interpreting results, with QBO W-E range in temperature
798 anomalies of ~1-2.5 K. The detailed agreement in shape and magnitude for the MERRA-2 and
799 ERA-Interim results for QBO W-E temperatures for each season supports the likelihood that
800 these QBO signals are real.

801 Further information was gained from the modern data sets regarding the equinoctial
802 seasons and modification of the SWJs. New results include 1) the existence of statistically
803 significant QBO zonal wind and temperature anomalies in the upper troposphere, 2) a more
804 complete, quantitative representation of the relationship among QBO temperature, zonal wind,
805 and the MMC as a function of season, 3) a time mean QBO structure diagram quantified by
806 latitude, altitude, and amplitude, 4) evidence that the subtropical signal is largest during JJA in
807 the SH, is large during MAM in both hemisphere, and is moderate in the NH during DJF, 5)
808 evidence that the eastward flow in the upper troposphere over the Pacific Ocean (Walker
809 circulation) is reduced by ~5-10 m/s during QBO W in MAM.

Accumulation of observational knowledge about QBO effects on the tropical and subtropical TTL over the past 60 years has led to a more complete and quantified picture. Independent results for QBO W-E tropopause temperature confirm findings that the QBO signal tends to be larger in areas of tropical deep convection. Since observational analyses persistently indicate the existence of a "direct effect" of the QBO on the UTLS, it is worthwhile to consider possible physical mechanisms which could explain the coupling.

7.2. Mechanisms for a "direct effect" of the QBO

The observations reviewed here suggest that a primary physical process involved is simply that the zonal mean temperature anomalies are fundamentally associated with the wave-driven QBO MMC, including anti-phasing between the tropics and subtropics, and the existence of QBO anomalies extending into the upper troposphere. This seems to be the primary physical cause of zonal mean QBO anomalies in the UTLS. Yet the enhanced QBO signal near areas of chronic deep convection and the influence on the Walker circulation argue in favor of an effect on deep convection. Collimore et al. (2003) reported that deep convection, as indicated by OLR and HRC, is enhanced over Amazonia, Africa, and Indonesia during QBO E and diminished during QBO W. Other authors report a diminution of rainfall over Indonesia during QBO W (Liess and Geller 2012; Anstey et al. 2020).

Three hypotheses have emerged in the literature which suggest physical mechanisms linking the QBO to deep convection, which are related to TTL temperature and thermodynamic efficiency, UTLS vertical wind shear, and UTLS inertial stability.

1) TTL temperature. Emanuel (1986) suggested that the thermodynamic efficiency of organized deep convection may be enhanced if the tropopause is higher and colder. Gray et al.

833 (1992b), Giorgetta et al. (1999), and others have suggested that the QBO modulates the static
834 stability environment of deep convection in the UTLS, leading to the promotion or inhibition of
835 convective strength and vertical penetration. If a cold QBO anomaly lies in the TTL,
836 convective complexes may grow more efficiently, penetrating to greater altitudes, locally
837 amplifying the zonal mean QBO cold anomaly.

838 *2) UTLS wind shear*. The influence of QBO-induced differences in vertical wind shear in
839 the UTLS on the development of deep convection and tropical cyclones has been explored by
840 Gray (1968), McBride and Zehr (1981), Gray and Scheaffer (1991), Gray et al. (1992a, b),
841 DeMaria and Kaplan (1994), and DeMaria (1996), and Frank and Ritchie (1999). They argue
842 that increased wind shear in the UTLS tends to dynamically disrupt deep convection.

843 *3) UTLS inertial stability*. Merrill (1989) suggested that the strength of a tropical cyclone
844 can be enhanced by weak inertial stability (reduced lateral resistance) in the UTLS outflow layer.
845 Montgomery and Farrell (1993) and Mecikalski and Tripoli (1998) found that mass divergence is
846 facilitated in quadrants of tropical cyclones where inertial stability is reduced.

847 Giorgetta et al. (1999) imposed QBO wind shear regimes in the UTLS in the ECHAM4
848 general circulation model and found that QBO E favors more cloudiness over Indonesia. Their
849 stated hypothesis is that the MMC associated with the imposed QBO anomalies created UTLS
850 temperature anomalies, which modified the static stability environment (Grise et al. 2010), and
851 were amplified by deep cloud feedback, supporting hypothesis 1).

852 In considering the observed signal, with regard to an amplified QBO effect over areas of
853 tropical deep convection, maxima in QBO W-E tropopause temperature amplitude tends to
854 coincide with areas of deep convection. However, the climatological centers of 70 - 150 hPa
855 westerly shear (Fig. 16) and climatological centers of 150 hPa easterly winds (Fig. 19) also tend

856 to coincide with regions of chronic deep convection. The fact that the TTL exhibits time mean
857 easterlies over Amazonia, Africa, and Indonesia may be related to the existence of deep
858 convection, which can transport easterly momentum from the trade winds to the UTLS. This
859 structure is also compatible with the steady-state "Gill solution" for planetary wave structure in
860 the tropical UTLS associated with a center of tropical heating (Gill, 1980), where westward flow
861 is expected over and to the west of an area of deep convection (see their Fig. 1 for equatorially-
862 centered convection and Fig. 3 for off-equatorial convection, similar to over Southeast Asia
863 during JJA). An imposed QBO W shear anomaly would increase the shear in the UTLS over
864 convective centers, under hypothesis 2) tending to "disrupt" the vigor of convection, while QBO
865 E would decrease the shear in the UTLS, promoting the robustness of convection.
866 The geographical distribution of the QBO signal in tropical TTL temperature is
867 compatible with an amplification during QBO E when the TTL is cold and UTLS shear is
868 reduced, and diminution during QBO W when the TTL is warm and UTLS shear is enhanced.
869 This tropical regime should be contrasted with the subtropical UTLS environment of tropical
870 cyclones, where typical easterly shears prevail (Figs. 16e-h, 19e-h), and QBO W can, in some
871 regions and seasons, diminish UTLS shear and enhance it in others.
872 This simple geographical comparison supports the idea that tropical deep convection may
873 act as a positive feedback mechanism on a QBO zonal mean temperature anomaly, in concert
874 with changes in TTL wind shear, through an increase (QBO E) or decrease (QBO W) in the
875 efficiency of tropical deep convection. Due to the importance of the tropics to global weather
876 and climate, it is of interest to study the QBO "direct effect" in more detail from modeling,
877 theoretical and observational points of view, to better understand the cause of these phenomena.
878

879 *Acknowledgments*. We would like to thank Stefan Hastenrath for providing tables of Berson's
880 data, Amihan Huesmann for creating Figs. 14-16, Shellie Rowe for help with refining the
881 figures, and the Editor and two anonymous reviewers for helpful suggestions. MHH
882 acknowledges support from NSF grants AGS-1555851 and AGS-1947658. This review is a
883 contribution to the SATIO-TCS (Stratospheric and Tropospheric Influences on Tropical
884 Convective Systems) initiative in SPARC (Stratosphere-troposphere Processes and their Role in
885 Climate).
886
887
888 **References**
889
890 Andrews, D. G., J. R. Holton, and C. B. Leovy, 1987, Middle Atmosphere Dynamics, 489
891 pp., Academic Press, San Diego, Calif.
892 Angell, J. K., and J. Korshover, 1964: Quasi-biennial variations in temperature, total ozone, and
893 tropopause height. *J. Atmos. Sci.*, **21**, 479-492.
894 Angell, J. K., J. Korshover, and G. F. Cotten, 1969: Quasi-biennial variations in the "centers of
895 action". *Mon. Wea. Rev.*, **97**, 867-872.
896 Angell, J. K., and J. Korshover, 1970: Quasibiennial, annual, and semiannual zonal wind and
897 temperature harmonic amplitudes and phases in the stratosphere and low mesosphere of
898 the Northern Hemisphere. *J. Geophys. Res.*, **75**, 543-550.
899 Angell, J. K., and J. Korshover, 1974: Quasibiennial and long-term temperature fluctuations in
900 tropopause pressure and temperature, and the relation to stratospheric water vapor
901 content. *Mon. Wea. Rev..,* **102**, 29-34.

902 Anstey, J. A., and T. G. Shepherd, 2014: High-latitude influence of the quasi-biennial
903 oscillation. *Quart. J. Roy. Meteorol. Soc*., **140**, 1–21.
904 Anstey, J. A., et al., 2020: Chapter 9: Quasi-biennial oscillation, Stratosphere-troposphere
905 Processes And their Role in Climate, (SPARC) Reanalysis Intercomparison Project (S-
906 RIP) report, 147 pp., in preparation.
907 Attard, H. E., and L. Coy, 2019: Connections between the stratosphere and synoptic variability,
908 *US CLIVAR Variations*, **17**, 1-6.
909 Baldwin, M. P., and T. J. Dunkerton, 1999: Propagation of the Arctic Oscillation from
910 the stratosphere to the troposphere. *J. Geophys. Res*., **104**, 30,937-30,946.
911 Baldwin, M. P., and Coauthors, 2001: The quasi-biennial oscillation. *Rev. Geophys*., **39**, 179–
912 229.
913 Berrisford, P., P. Kallberg, S. Kobayashi, D. P. Dee, S. M. Uppala, A. J. Simmons, P. Poli, 2011:
914 "Atmospheric conservation properties in ERA-Interim", ERA Report Series, ECMWF,
915 Reading, UK.
916 Berson, A., 1910: Bericht über die aerologische expedition nach Ostfrika im Jahre 1908,
917 erstattet von ihrem Leiter Arthur Berson, Braunschweig, 119 pp. (K. Preussisches
918 aeronaut. Observatorium bei Lindenberg.)
919 Boville, B. A., 1984: The influence of the polar night jet on the tropospheric circulation in a
920 GCM. *J. Atmos. Sci*., **41**, 1132-1142.
921 Brönniman, S. and A. Stickler, 2013: Aerological observations in the tropics in the early
922 twentieth century. *Meteorologische Zeitschrift*, **22**, 349–358
923 Camargo, S.J., and A.H. Sobel, 2010: Revisiting the influence of the quasi-biennial oscillation
924 on tropical cyclone activity. *J. Climate*, **23**, 5810-5825.

925 Choi, W., et al., 2002: On the secondary meridional circulation associated with the quasi-
926 biennial oscillation. *Tellus*, **54B**, 395–406.
927 Collimore, C. C., M. H. Hitchman, and D. W. Martin, 1998: Is there a quasi-biennial oscillation
928 in tropical convection? *Geophys. Res. Letts*., **25**, 333-336.
929 Collimore, C. C., D. W. Martin, M. H. Hitchman, A. Huesmann, and D. Waliser, 2003: On the
930 relationship between the QBO and tropical deep convection. *J. Climate*, **16**, 2552-2568.
931 Coy, L., P. A. Newman, S. Pawson, and L. R. Lait, 2017: Dynamics of the disrupted 2015/16
932 Quasi-Biennial Oscillation. *J. Clim.*, **30**, 5661–5674.
933 Dee, D, P., 2011: The ERA-Interim reanalysis: configuration and performance of the data
934 assimilation system. *Q. J. R. Meteorol. Soc.,* **137**, 553–597.
935 DeMaria, M., 1996: The effect of vertical shear on tropical cyclone intensity change. *J. Atmos.*
936 *Sci*., **53**, 2076-2087.
937 DeMaria, M., and J. Kaplan, 1994: A statistical hurricane intensity prediction scheme (SHIPS)
938 for the Atlantic basin. *Wea. Forecasting*, **9**, 209-220.
939 Dessler, A. E., S. P. Palm, and J. D. Spinhirne, 2006: Tropical cloud-top height distributions
940 revealed by the Ice, Cloud, and Land Elevation Satellite (ICESat)/Geoscience Laser
941 Altimeter Systerm (GLAS). *J. Geophys. Res.,* **111**, D12215.
942 Dickinson, R. E., 1968: On the excitation and propagation of zonal winds in an atmosphere with
943 Newtonian cooling. *J. Atmos. Sci.*, **25**, 269-279.
944 Dunkerton, T. J., 1983: Laterally-propagating Rossby waves in the easterly acceleration phase of
945 the quasi-biennial oscillation. *Atmosphere-Ocean*, **21**, 55-68.
946 Dunkerton, T. J., 2017: Nearly identical cycles of the quasi-biennial oscillation in the equatorial
947 lower stratosphere. *J. Geophys. Res.-Atmos*., **122**, 8467–8493.

948 Eluszkiewicz, J., et al., 1996: Residual circulation in the stratosphere and lower mesosphere and
949 diagnosed from Microwave Limb Sounder data. *J. Atmos. Sci.*, **53**, 217-240.
950 Emanuel, K.A., 1986: An air-sea interaction theory for tropical cyclones. Part I: Steady state
951 maintenance. *J. Atmos. Sci*., **43**, 585-604.
952 Folkins, I., M. Loewenstein, J. Pokolske, S. J. Oltmans, and M. Profitt, 1999: A 14 km mixing
953 barrier in the tropics: Evidence from ozonesondes and aircraft measurements. *J*.
954 *Geophys*. *Res*., **104**, 22,095-22,102.
955 Fraedrich, K., S. Pawson, and R. Wang, 1993: An EOF analysis of the vertical-time delay
956 structure of the quasi-biennial oscillation. *J*. *Atmos*. *Sci*., **50**, 3357-3365.
957 Frank, W. M., and E. A. Ritchie, 1999: Effects of environmental flow upon tropical cyclone
958 structure. *Mon*. *Wea*. *Rev*., **127**, 2044-2061.
959 Fueglistaler, S., A. E. Dessler, T. J. Dunkerton, I. Folkins, Q. Fu, and P. W. Mote (2009),
960 Tropical tropopause layer. *Rev*. *Geophys*., **47**, RG1004.
961 Garfinkel, C.I., and D.L. Hartmann, 2007: Effects of the El Niño–Southern Oscillation and the
962 Quasi-Biennial Oscillation on polar temperatures in the stratosphere. *J. Geophys. Res*.,
963 **112**, D19112.
964 Garfinkel, C.I., and D.L. Hartmann, 2011: The influence of the quasi-biennial oscillation on the
965 troposphere in winter in a hierarchy of models. Part I: Simplified dry GCMs. *J. Atmos.*
966 *Sci.*, **68**, 1273-1289.
967 Gettelman, A., and P. M. de F. Forster, 2002: A climatology of the tropical tropopause layer. *J.*
968 *Meteorol. Soc. Jpn*., **80, 4B**, 911-924.
969 Gettelman, A., M. L., Salby, and F. Sassi, 2002: Distribution and influence of convection in the
970 tropical tropopause region. *J*. *Geophys*. *Res*., **107**, 4080.

971 Gille, J. C., and J. M. Russell III, 1984: The Limb Infrared Monitor of the Stratosphere (LIMS)
972 experiment description, performance, and results. *J. Geophys. Res.*, **89**, 5125-5140.
973 Gill, A. E., 1980: Some simple solutions for heat-induced tropical circulation. *Quart. J. R.*
974 *Meteorol. Soc.*, **106**, 447-462.
975 Giorgetta, M.A., L. Bengtsson, and K. Arpe, 1999: An investigation of QBO signals in the east
976 Asian and Indian monsoon in GCM experiments. *Clim. Dyn.*, **15**, 435-450.
977 Gray, W. M., 1968: Global view of the origin of tropical disturbances and storms: *Mon. Wea.*
978 *Rev.*, **96**, 669-700.
979 Gray, W.M., 1984: Atlantic seasonal hurricane frequency. Part I: El Niño and 30 mb quasi-
980 biennial oscillation influences. *Mon. Wea Rev.*, **112**, 1649-1668.
981 Gray, W. M, and J. D. Sheaffer, 1991: El Nino and QBO influences on tropical cyclone activity,
982 pp. 258-284, in *Teleconnections Linking Worldwide Climate Anomalies*, Cambridge
983 University Press, M. Glantz, R. W. Katz and N. Nicholls, Eds.
984 Gray, W. M., C. W. Landsea, P. W. Mielke Jr., and K. J. Berry, 1992a: Predicting Atlantic
985 seasonal hurricane activity 6-11 months in advance. *Weather Forecasting*, **7**, 440-455.
986 Gray, W. M., J. D. Scheaffer, and J. A. Knaff, 1992b: Influence of the stratospheric QBO on
987 ENSO variability. *J. Meteorol. Soc. Jpn.,* **70**, 975-995.
988 Gray, L. J., J. A. Anstey, Y. Kawatani, H. Lu, S. Osprey, and V. Schenzinger, 2018: Surface
989 impacts of the Quasi Biennial Oscillation. *Atmos. Chem. Phys.*, **18**, 8227–8247.
990 Grise, K. M., D. W. J. Thompson, and T. Birner, 2010: A global survey of static stability in the
991 stratosphere and upper troposphere. J. *Atmos. Sci.*, **23**, 2275-2292.
992 Hamilton, K., 2012: Sereno Bishop, Rollo Russell, Bishop's Ring and the Discovery of the
993 "Krakatoa Easterlies", *Atmos.-Ocean*, **50**, 169-175,

994 Hastenrath, S., 1990: The relationship of highly reflective clouds to tropical climate anomalies. *J.*
995 *Climate*, **3**, 353–365.
996 Hastenrath, S., 2007: Equatorial zonal circulations: Historical perspectives. *Dyn. Atmos. Oceans*,
997 **43**, 16–24.
998 Haynes, P. H., P. Hitchcock, M. H. Hitchman, S. Yoden, H. Hendon, G. Kiladis, K. Kodera, and
999 I. Simpson, 2020: Stratosphere-troposphere coupling in the tropics. *J. Meteorol. Soc.*
1000 *Jpn.*, in review.
1001 Highwood, E. J., and B. J. Hoskins, 1998: The ·tropical tropopause. *Quart. J. Roy. Meteor. Soc.*,
1002 **124**, 1579-1604.
1003 Hitchman, M. H. and C. B. Leovy, 1986: Evolution of the zonal mean state in the equatorial
1004 middle atmosphere during October 1978 - May 1979. *J. Atmos. Sci.*, **43**, 3159-3176.
1005 Hitchman, M. H., M. McKay, and C. R. Trepte, 1994: A climatology of stratospheric aerosol. *J.*
1006 *Geophys. Res.*, **99**, 20,689-20,700.
1007 Hitchman, M. H., and A. S. Huesmann, 2009: Effect of the Quasibiennial Oscillation on Rossby
1008 Wave breaking in the stratosphere and tropopause layer. *J. Atmos. Sci.*, **66**, 935-946.
1009 Ho, C.-H., et al., 2009: Influence of stratospheric quasi-biennial oscillation on tropical cyclone
1010 tracks in the western North Pacific. *Geophys. Res. Letts.*, **36**, L06702, doi:
1011 10.1029/2009GL037163.
1012 Hoerling, M. P., T. D. Schaack, and A. J. Lenzen, 1991: Global objective tropopause analysis.
1013 *Mon. Wea. Rev.*, **119**, 1816-1831.
1014 Hoinka, K. P., 1998: Statistics of the global tropopause pressure. *Mon. Wea. Rev.*, **126**,
1015 3303-3325.

1016 Hoinka, K. P., 1999: Temperature, humidity, and wind at the global tropopause pressure. *Mon.*
1017 *Wea. Rev.*, **127**, 2248-2265.
1018 Holton, J. R., and C.-H. Tan, 1980: The influence of the equatorial quasibiennial oscillation on
1019 the global circulation at 50 mb. *J. Atmos. Sci.*, **37**, 2200–2208.
1020 Huesmann, A., and M. H. Hitchman, 2001: The stratospheric quasi-biennial oscillation in the
1021 NCEP reanalysis: Climatological structures. *J. Geophys. Res.*, **106**, 11,859-11870.
1022 Huesmann, A. S., and M. H. Hitchman, 2003: The 1978 shift in the NCEP reanalysis
1023 stratospheric quasibiennial oscillation. *Geophys, Res. Letts.*, **30**, 2, 1048.
1024 Kalnay, E., et al., 1996: The NCEP /NCAR 40 year reanalyses project. *Bull. Amer. Meterol. Soc.*,
1025 **77**, 437-471.
1026 Kane, R. P., 1995: Quasi-biennial and quasi-triennial oscillations in the summer monsoon
1027 rainfall of the meteorological subdivisions of India. *Mon. Weather Rev.,* **123**, 1178-1184.
1028 Kawatani, Y., K. Hamilton, K. Miyazaki, M. Fujiwara, and J. A. Anstey, 2016: Representation
1029 of the tropical stratospheric zonal wind in global atmospheric reanalyses. *Atmos. Chem.*
1030 *Phys.*, **16**, 6681-6699.
1031 Kinnersley, J. S., 1999: Seasonal asymmetry of the low- and middle-latitude QBO circulation
1032 anomaly. *J. Atmos. Sci.*, **56**, 1140-1153.
1033 Kistler, R., et al., 2001: The NCEP-NCAR 50-year reanalysis: monthly means CD-ROM and
1034 documentation. *Bull. Amer. Meteorol. Soc.,* **82**, 247-267.
1035 Knaff, J. A., 1993: Evidence of a stratospheric QBO modulation of tropical convection. Dept. of
1036 Atmospheric Science, Colorado State University, Fort Collins, CO, Paper 520, 91 pp.
1037 Lindzen, R. S., and J. R. Holton, 1968: A theory of the quasi-biennial oscillation. *J. Atmos. Sci.*,
1038 **25**, 1095-1107.

1039 Liess, S., and M. A. Geller, 2012: On the relationship between QBO and distribution of tropical
1040 deep convection. *J. Geophys. Res.*, **117**, D03108.
1041 Lu, H., M. H. Hitchman, L. J. Gray, J. Anstey, and S. M. Osprey, 2020: On the role of Rossby
1042 wave breaking in the quasi-biennial modulation of the stratospheric polar vortex during
1043 boreal winter. *Quart. J. Royal Meteorol. Soc.,* **146 (729)**, 1939-1959.
1044 Martin, Z., A. Sobel, and S. Wang, 2020: Variability in QBO temperature anomalies in the TTL
1045 on annual and decadal time scales. *J. Clim., under revision*.
1046 Match, A., and S. Fueglistaler, 2019: The buffer zone of the quasi-biennial oscillation. *J. Atmos.*
1047 *Sci.*, **76**, 3553-3567.
1048 McBride, J. L., and R. Zehr, 1981: Observational analysis of tropical cyclone formation. Part II:
1049 Comparison of non-developing versus developing systems. *J. Atmos. Sci.,* **38**, 1132-
1050 1151.
1051 McCormick, M.P., J. M. Zawodny, R. E. Veiga, J. C. Larsen, and P. H. Wang, 1989: An
1052 overview of SAGE I and SAGE II ozone measurements. *Planet. Space Sci.*, **37**, 1567-
1053 1586.
1054 Mecikalski, J. R. and G. J. Tripoli, 1998: Inertial available kinetic energy and the dynamics of
1055 tropical plume formation. *Mon. Wea. Rev.*, **126**, 2200-2216.
1056 Merrill, R. T., 1989: Environmental influences on hurricane intensification. *J. Atmos. Sci.*, **45**,
1057 1678-1687.
1058 Montgomery, M.T., and B. F. Farrell, 1993: Tropical cyclone formation. *J. Atmos. Sci.,* **50**, 285-
1059 310.

1060 Newell, R. E., J. W. Kidson, D. G. Vincent and G. J. Boer, 1974: *The general circulation of the*
1061 *tropical atmosphere and interactions with extratropical latitudes. Volume 2.* MIT Press,
1062 Cambridge, Mass., pp. 371.
1063 Newman, P. A., L. Coy, S. Pawson, and L. R. Lait, 2016: The anomalous change in the QBO in
1064 2015–2016. *Geophys. Res. Lett*., **43**, 8791–8797.
1065 Osprey, S. M., et al., 2016: An unexpected disruption of the atmospheric quasi-biennial
1066 oscillation. *Science*, **353**, 1424-1427.
1067 Pawson, S. and M. Fiorino, 1999: A comparison of reanalyses in the tropical stratosphere. Part
1068 3: Inclusion of the pre-satellite data era. *Climate Dyn.,* **15**, 241-250.
1069 Pena-Ortiz, C., P. Ribera, R. Garcia-Herrera, M. A. Giorgetta, and R. R. Garcia, 2008: Forcing
1070 mechanism of the seasonally asymmetric quasi-biennial oscillation secondary circulation
1071 in ERA-40 and MAECHAM5. *J. Geophys. Res*., **113**, D16103.
1072 Plumb, R.A., and R.C. Bell, 1982: A model of the quasi-biennial oscillation on an equatorial
1073 beta-plane. *Quart. J. Roy. Meteor. Soc*., **108**, 335-352.
1074 Randel, W. J., F. Wu, R. Swinbank, J. Nash, and A. O'Neill, 1999: Global QBO circulation
1075 derived from UKMO stratospheric analyses. *J. Atmos. Sci.,* **56**, 457-474.
1076 Randel, W. J., F. Wu, and D. J. Gaffen, 2000: Interannual variability of the tropical tropopause
1077 derived from radiosonde data and NCEP reanalyses. *J. Geophys. Res.,* **105**, 15,509-
1078 15,523.
1079 Reid, G. C., and K. S. Gage, 1985: Interannual variations in the height of the tropical tropopause.
1080 *J, Geophys. Res.,* **90**, 5629-5635.
1081 Reid, G. C., 1994: Seasonal and interannual temperature variations in the tropical stratosphere.
1082 *J. Geophys. Res.*, **99 (D9)**, 18,923-18,932.

1083 Reed, R. J., W. J. Campbell, L. A. Rasmusson, and D. G. Rogers, 1961: Evidence of the
1084 downward-propagating annual wind reversal in the equatorial stratosphere. *J. Geophys.*
1085 *Res*., **66**, 813-818.
1086 Reed, R. J., 1966: Zonal wind behavior in the equatorial stratosphere and lower mesosphere. *J.*
1087 *Geophys. Res.*, **71**, 4223-4233.
1088 Russell, P. B., et al., 1981: Satellite and correlative measurements of the stratospheric aerosol,
1089 II, Comparison of measurements made by SAM II, dustsondes and an airborne lidar. *J.*
1090 *Atmos. Sci.,* **38**, 1295-1312.
1091 Seidel, D. J., R. J. Ross, and J. K. Angell, 2001: Climatological characteristics of the
1092 tropical tropopause as revealed by radiosondes. *J. Geophys. Res*., **106**, 7857-7878.
1093 Seol, D.-I., and K. Yamazaki, 1998: QBO and Pinatubo signals in the mass flux at 100 hPa and
1094 stratospheric circulation. *Geophys. Res. Letts*., **25**, 1641-1644.
1095 Simkin, T., and R. S. Fiske, 1984: *Krakatau 1883, The Volcanic Eruption and Its Effects.*
1096 Washington, D.C., Smithsonian Institution Press, 464 pp.
1097 Tegtmeier, S., et al., 2020: Temperature and tropopause characteristics from reanalysis data in
1098 the tropical tropopause layer. *Atmos. Chem. Phys*., **20**, 753-770.
1099 Thompson, D. W. J., and J. M. Wallace, 2001: Regional climate impacts of the Northern
1100 Hemisphere annular mode. *Science*, **293**, 85–89.
1101 Trepte, C. R., and M. H. Hitchman, 1992: Tropical stratospheric circulation diagnosed in
1102 satellite aerosol data. *Nature*, **355**, 626-628.
1103 Trepte, C. R., 1993: *Tracer Transport in the Tropical Lower Stratosphere.* Ph.D. dissertation,
1104 University of Wisconsin – Madison, 160 pp. Web: https://www.osti.gov/biblio/404799-
1105 tracer-transport-tropical-lower-stratosphere-ph-thesis.

1106 Tuck, A. F., J. M. Russell III, J. E. Harries, 1993: Stratospheric dryness: Antiphased desiccation
1107 over Micronesia and Antarctica. *Geophys. Res. Letts.,* **20**, 1227-1230.
1108 Tucker, G. B., and J. M. Hopwood, 1968: The 26-month zonal wind oscillation in the lower
1109 stratosphere of the Southern Hemisphere. *J. Atmos*., **25**, 293-298.
1110 Veryard, R. G., and R. A. Ebdon, 1961: Fluctuations in tropical stratospheric winds. *Meteor*.
1111 *Mag*., **90**, 125-143.
1112 Virts, K. S., J. M. Wallace, Q. Fu, and T. P. Ackerman, 2010: Tropical tropopause transition
1113 layer cirrus as represented by CALIPSO lidar observations. *J. Atmos. Sci.,* **67**, 3113-
1114 3129.
1115 Wallace, J. M., 1967: A note on the role of mean meridional motions in the biennial wind
1116 oscillation. *Quart. J. Roy. Meteor. Soc*., **93**, 176-185.
1117 Wallace, J. M., 1973: General circulation of the tropical lower stratosphere. *Rev. Geophys.*
1118 *Space Phys*., **11**, 191–222.
1119 Wallace, J. M., R. L. Panetta, and J. Estberg, 1993: Representation of the equatorial
1120 stratospheric quasi-biennial oscillation in EOF space. *J. Atmos. Sci*., **50**, 1751 – 1762.
1121 Wang, J., H.-M. Kim, and E.K.M. Chang, 2018: Interannual modulation of Northern
1122 Hemisphere winter storm tracks by the QBO. *Geophys. Res. Letts*., **45**, 2786–2794.
1123 Webster, P. J., and J. R. Holton, 1982: Cross-equatorial response to midlatitude forcing in a
1124 zonally-varying basic state. *J. Atmos. Sc*i., **39**, 722-733.
1125 Winchester, S., 2003: *Krakatau - The Day The World Exploded: 27 August 1883*, Viking Press,
1126 448 pp.
1127 Yang, H., and K. K. Tung, 1996: Cross-isentropic stratosphere-troposphere exchange of mass
1128 and water vapor. *J. Geophys. Res*., **101**, 9413-9423.

Yasunari, T., 1989: A possible link of the QBOs between the stratosphere, troposphere and sea surface temperature in the tropics. *J. Meteor. Soc. Jpn.,* **67**, 483-493.

Zhou, X.-L., M.A. Geller, and M.-H. Zhang, 2001: Tropical cold point tropopause characteristics derived from ECMWF reanalyses and soundings. *J. Clim.*, **14**, 1823-1838.

Figure Captions

Figure 1. Time – altitude section of monthly mean zonal wind (contour interval 5 m/s) at Canton Island (3°S, 172°W) in the altitude layer 15-30 km during the period March 1955 – March 1960. Layer-averaged wind speeds (in m/s, with a space instead of a decimal point) are plotted to the left of vertical lines, while the number of observations in each mean is shown to the right (after Fig. 1 of Reed et al. 1961).

Figure 2. Twelve month running average of monthly mean 50 hPa temperatures for stations approximately evenly spaced north and south of the equator, in the range 80°N – 76°S, during 1957-1962. The scale for 1°C is shown in the lower left inset. Short vertical tick marks correspond to the beginning of a year. Thin blue vertical lines were added to indicate QBO temperature extrema at Canton Island (after Fig. 3 of Angell and Korshover 1964).

Figure 3. Left (Fig. 3 of Dickinson 1968): "Schematic depiction of the kinematics of the theoretical downward progression of a biennial wave centered at the equator, showing easterlies overlying westerlies". The nature of the momentum forcing was not yet clear. Right (Fig. 1 of Plumb and Bell 1982): "Schematic representation of the mean meridional circulation driven by an equatorial thermal anomaly, and the consequent acceleration of the mean zonal wind (in part,

after Reed (1964) and Dickinson (1968)). Solid contours: potential isotherms. Dashed contours: Isopleths of zonal velocity. +/- : Sign of zonal acceleration. (a) Warm anomaly (b) Cold anomaly". In their 2D model, the circulation is obtained by parameterizing the absorption of eastward and westward-travelling equatorial waves in the zonal momentum equation. Note the anti-phasing of temperature anomalies in the subtropics and tropics implied by the MMC.

Figure 4. Twelve-month running mean tropopause heights at five Micronesian stations (left panel, after Fig. 2 of Reid and Gage 1985) and for more widely separated stations, including Curacao and Ascension Island in the Atlantic (right panel, after Fig. 3 of Reid and Gage 1985), where arrows at the top identify peaks that occur at more than one station. The 16-km level is indicated for each curve at left. Thin blue vertical lines were added at the beginning of each even year.

Figure 5. Left: coherence spectrum of monthly mean zonal wind between 50 and 700 hPa at Singapore. Right: individual power spectra at 50 and 700 hPa for the 18-yr period 1963-1981. Power spectrum units plotted are in m/s per month and a maximum lag of 40 was used. Note that the power scale for 50 hPa is 10 times that for 700 hPa. Thin blue vertical lines were added to the power spectra to highlight the band ~22-36 months (adapted from Fig. 3 of Yasunari 1989).

Figure 6. Latitude-altitude sections of zonal mean LIMS a) temperature (contour interval 5 K), b) zonal wind (interval 10 m/s) and c) normalized absolute vorticity (see text, contour interval 1 day^{-1}) for the period 31 October – 5 November 1978. Values of temperature and zonal wind

1175 have been smoothed with a 1-2-1 filter in latitude. Schematic arrows indicate the MMC which is
1176 compatible with the observed patterns in temperature and PV and with theoretical models. (Fig.
1177 4 of Hitchman and Leovy 1986. © American Meteorological Society. Used with permission.)
1178
1179 Figure 7. Latitude-altitude sections of aerosol extinction ratio at 1 um during two 40-day periods
1180 representative of two different phases of the QBO: a) dominant westerly shear centered at 11
1181 November 1984 (contour interval 2.5) and b) dominant easterly shear, centered at 4 October
1182 1988 (contour interval 0.5). Crosses indicate locations of the daily average of ~15 profiles.
1183 Arrows indicate the inferred QBO circulation based on the aerosol distribution. The tropopause
1184 is indicated with a dotted line. The latitudes for the eruptions of Mt. Ruiz in November 1985 and
1185 of Mt. Pinatubo in June 1991 are indicated by "R" and "P", respectively, both of which occurred
1186 during easterly shear in the lower stratosphere. The altitude of the zero-wind line at the equator
1187 is shown at the right of each section. (Figure 3 of Trepte and Hitchman 1992).
1188
1189 Figure 8. QBO W-E differences in SAGE aerosol extinction ratio (contour interval 5%), using
1190 the 50-70 hPa wind shear index, based on 10 years (1979-1981 and 1984-1990) of SAGE I and II
1191 and SAM II aerosol measurements. Dashed contours indicate higher aerosol during QBO E
1192 shear (Fig. 7 of Hitchman et al. 1994).
1193
1194 Figure 9. Schematic diagram of the QBO MMC and its relationship with anomalies of zonal
1195 mean temperature (solid contours), zonal velocity (dashed contours) and tropopause altitude
1196 (thick gray lines) for a) warm anomaly during descending QBO W regime and b) cold anomaly
1197 during descending QBO E regime approaching the UTLS (from Collimore et al. 2003, ©

American Meteorological Society, used with permission. Cf. similar diagrams in Gray et al. 1991b and Trepte 1993).

Figure 10. "Calculated temperature anomalies forced by the easterly and westerly phases of the quasi-biennial wind variation." A typical value for vertical shear of 3 m/s per 6 km and a mean equatorial temperature of 210 K were assumed, (Fig. 8 from Reid, 1994).

Figure 11. "Latitudinal structure of QBO variations in a) tropopause temperature (K per 10 m/s) and b) tropopause pressure (hPa per 10 m/s) for 1979-1997, derived from regression analysis. Curves show NCEP data, and circles indicate results for each radiosonde location. Error bars indicate +/-2 sigma statistical uncertainties. Units are Kelvins per 10 m/s of QBO winds at 50 hPa, which vary over ~+/-20 m/s during a QBO cycle" (Fig. 13 of Randel et al. 2000).

Figure 12. a) Latitudinal distribution of NCEP zonal mean tropopause temperature (K) for DJF QBO W (dotted line), QBO E (dashed line), and climatological mean (solid line). b) QBO W (dotted line) and QBO E (dashed line) departure from the annually averaged zonal mean tropopause temperature (K). Deviations from climatology in a) are exaggerated by a factor of 5 for clarity (Fig. 15 of Huesmann and Hitchman 2001).

Figure 13. a) Latitudinal distribution of NCEP 50-70 hPa zonal mean wind shear (m/s per 20 hPa) for DJF QBO W (dotted line), QBO E (dashed line), and climatological mean (solid line). b) QBO W (dotted line) and QBO E (dashed line) departure from the annually averaged 50 – 70 hPa wind shear (Fig. 9 of Huesmann and Hitchman 2001).

Figure 14. Seasonally-averaged (left, panels a-d): QBO W-E NCEP tropopause temperature (contour interval 0.3 K, dashed contours negative), and (right, panels e-h): NCEP mean tropopause temperature (contour interval 3 K in the shaded regions below 200 K, 4 K elsewhere), for DJF (panels a, b, e, f) and for JJA (panels c, d, g, h). NCEP data during 1958-1978 and 1979-2000 are shown separately for each season (upper and lower of each pair). In the QBO W-E difference fields (left), light shading indicates confidence level above 90%, dark shading above 95%, and the fields have been smoothed once with a 9-point square filter.

Figure 15. As in Fig. 14, except for NCEP tropopause pressure. In the QBO W-E plots (left, panels a-d), the contour interval is 1.5 hPa, with dashed contours negative, and light shading indicates confidence level above 90%, dark shading above 95%. In QBO seasonal mean plots (right, panels e-h), the contour interval is 10 hPa in the shaded region below 120 hPa, and 20 hPa elsewhere.

Figure 16. As in Fig. 14, except of NCEP 70 - 150 hPa zonal wind shear. In the QBO W-E plots (left, panels a-d) the contour interval is 1 m s^{-1} $(80\ hPa)^{-1}$, with dashed contours negative, and light shading indicates confidence level above 90%, dark shading above 95%. In seasonal mean plots (right, panels e-h), the contour interval is 5 m s^{-1} $(80\ hPa)^{-1}$, with positive values shaded.

1242 Figure 17. QBO W-E range in MERRA-2 CPT temperature (color bar, contour interval 0.125 K)
1243 for the 38-yr period 1980-2017, for a) the annual mean, b) DJF, c) MAM, d) JJA, and e) SON.
1244 Regions with less than 99% confidence are indicated in black.
1245
1246 Figure 18. Seasonal mean ERA-Interim 100 hPa temperature (left, panels a-d): QBO W-E
1247 differences (color bar, range -3 to 3 K, contour interval 0.25 K), and (right, panels e-h): seasonal
1248 means (color bar, range 188 to 218 K, contour interval 2 K), for DJF (a, e), MAM (b, f), JJA (c,
1249 g), and SON (d, h). Monthly mean data for the 40-yr period 1979 – 2018 were analyzed using
1250 the EOF method of Wallace et al. (1993). QBO W-E values shown are phase-4 minus phase-8,
1251 which corresponds W and E maxima in the lower stratosphere. Diagonal green lines indicate
1252 regions with less than 95% statistical significance. In the left-hand panels, the zero line, or node,
1253 is indicated with a dotted black line.
1254
1255 Figure 19. As in Fig. 18, except of (left, panels a-d): QBO W-E differences in 150 hPa zonal
1256 wind (color bar, range -10 to 10 m/s, contour interval 1 m/s) and (right, panels e-g): seasonal
1257 mean distribution of 150 hPa zonal wind (color bar, range -40 to 40 m/s, contour interval 5 m/s).
1258 The zero contour is represented with a dotted black line.
1259
1260 Figure 20. Seasonal mean ERA-Interim zonal mean QBO W-E (phase 4 minus phase 8
1261 differences) data for DJF (a, e), MAM (b, f), JJA (c, g), and SON (d, h), in the domain 0-50 km
1262 (1000 -1 hPa), 40°S-40°N, of (a-d) zonal wind (color bar, range -30 to 30 m/s, with contour
1263 interval 1 m/s until +/-5 m/s, and an interval of 5 m/s for larger values), and (e-g) temperature
1264 (color bar, range -5 to 5 K, interval 0.25 K until +/-1 K, and an interval of 1 K for larger values).

Reference vector scales of 1 mm/s for vertical motion and 20 cm/s for meridional motion are shown. The black dotted line is the zero contour. The yellow dotted lines separate regions of fine and coarse contour intervals. The heavy-dashed lime-green line indicates the seasonal mean tropopause. Monthly mean data for the 40-yr period 1979 – 2018 were analyzed with the EOF method of Wallace et al. (1993). Phases 4 and 8 correspond to QBO W and E maximizing in the lowest stratosphere. Diagonal green hatching indicates regions with less than 95% statistical significance. Vectors are not plotted if both components are not significant at the 95% level.

Figure 21. Time mean ERA-Interim QBO W-E differences during the 40-yr period 1979-2018, in the domain 0-50 km (1000 -1 hPa), 40°S-40°N, for a) zonal wind (color bar, range -30 to 30 m/s, with contour interval 1 m/s until +/-5 m/s, with interval 5 m/s for larger values), and b) temperature (color bar, range -5 to 5 K, interval 0.25 K until +/-1 K, with interval 1 K for larger values). The reference vector scales of 1 mm/s for vertical motion and 20 cm/s for meridional motion are shown. The black dotted line is the zero contour. The yellow dotted lines separate regions of fine and coarse contour intervals. The heavy-dashed lime-green line indicates the time mean tropopause. Monthly mean data were analyzed with the EOF method of Wallace et al. (1993). Phases 4 and 8 correspond to QBO W and E maximizing in the lowest stratosphere. Diagonal green hatching indicates regions with less than 95% statistical significance. Vectors are not plotted if both components are not significant at the 95% level. The climatological mean tropopause is indicated with a thick dashed gray line (~90 hPa in the tropics and ~250 hPa near 40°).

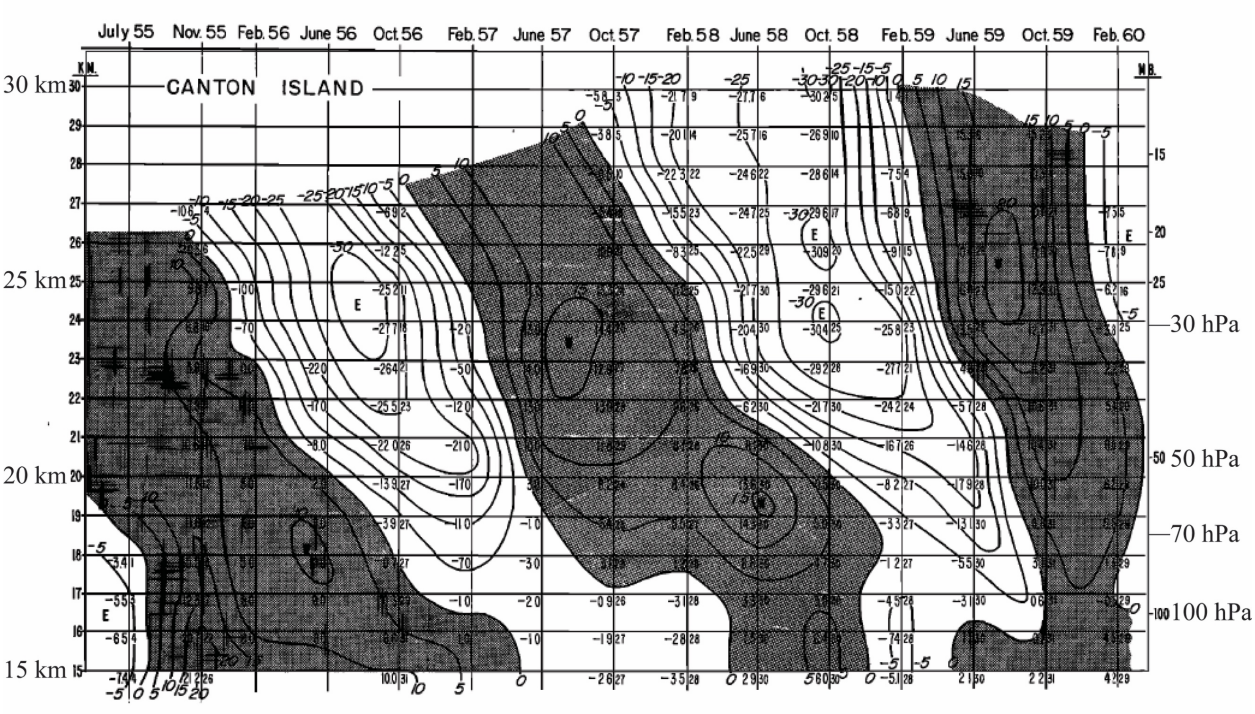

Figure 1. Time – altitude section of monthly mean zonal wind (contour interval 5 m/s) at Canton Island (3°S, 172°W) in the altitude layer 15-30 km during the period March 1955 – March 1960. Layer-averaged wind speeds (in m/s, with a space instead of a decimal point) are plotted to the left of vertical lines, while the number of observations in each mean is shown to the right (after Fig. 1 of Reed et al. 1961).

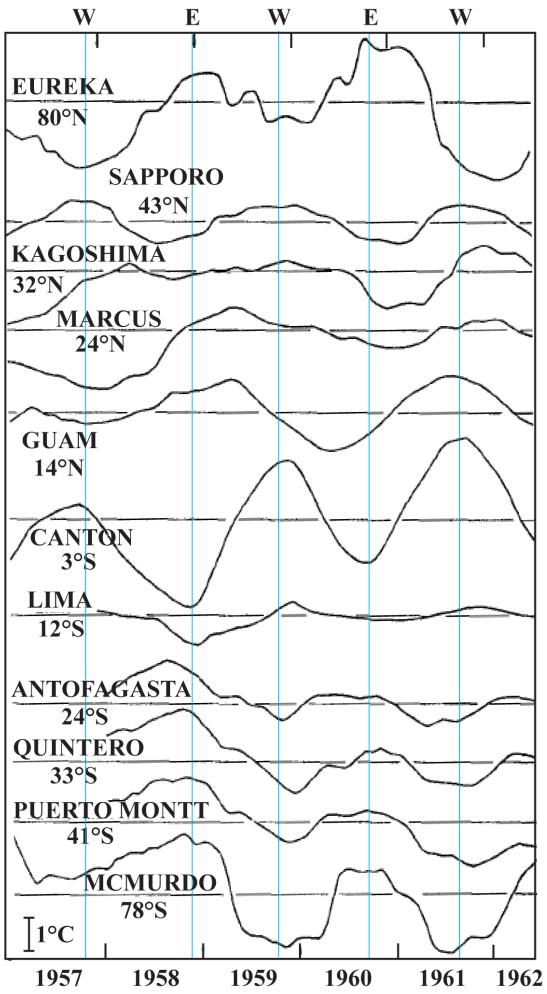

Figure 2. Twelve month running average of monthly mean 50 hPa temperatures for stations approximately evenly spaced north and south of the equator, in the range 80°N – 76°S, during 1957-1962. The scale for 1°C is shown in the lower left inset. Short vertical tick marks correspond to the beginning of a year. Thin blue vertical lines were added to indicate QBO temperature extrema at Canton Island (after Fig. 3 of Angell and Korshover 1964).

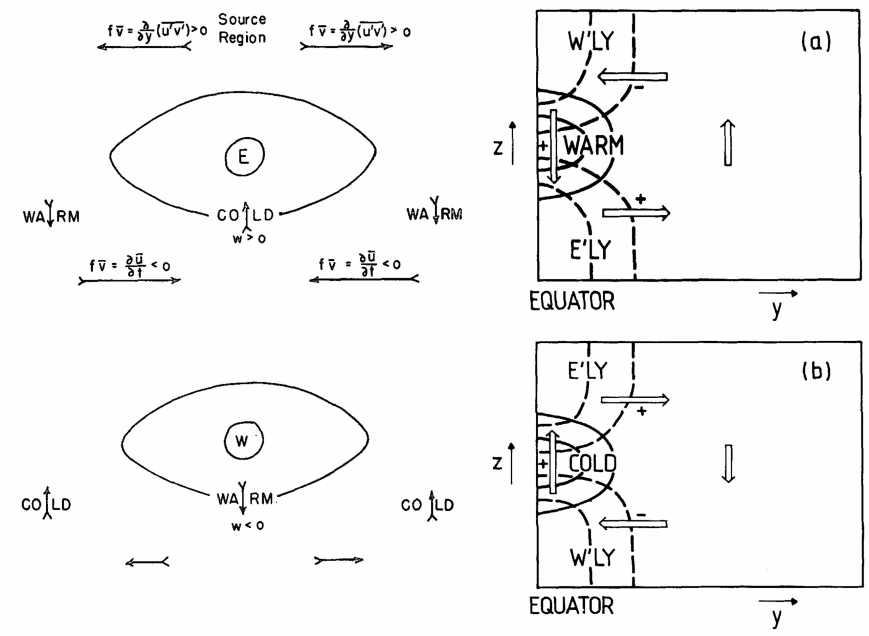

Figure 3. Left (Fig. 3 of Dickinson 1968): "Schematic depiction of the kinematics of the theoretical downward progression of a biennial wave centered at the equator, showing easterlies overlying westerlies". The nature of the momentum forcing was not yet clear. Right (Fig. 1 of Plumb and Bell 1982): "Schematic representation of the mean meridional circulation driven by an equatorial thermal anomaly, and the consequent acceleration of the mean zonal wind (in part, after Reed (1964) and Dickinson (1968)). Solid contours: potential isotherms. Dashed contours: Isopleths of zonal velocity. +/- : Sign of zonal acceleration. (a) Warm anomaly (b) Cold anomaly". In their 2D model, the circulation is obtained by parameterizing the absorption of eastward and westward-travelling equatorial waves in the zonal momentum equation. Note the anti-phasing of temperature anomalies in the subtropics and tropics implied by the MMC.

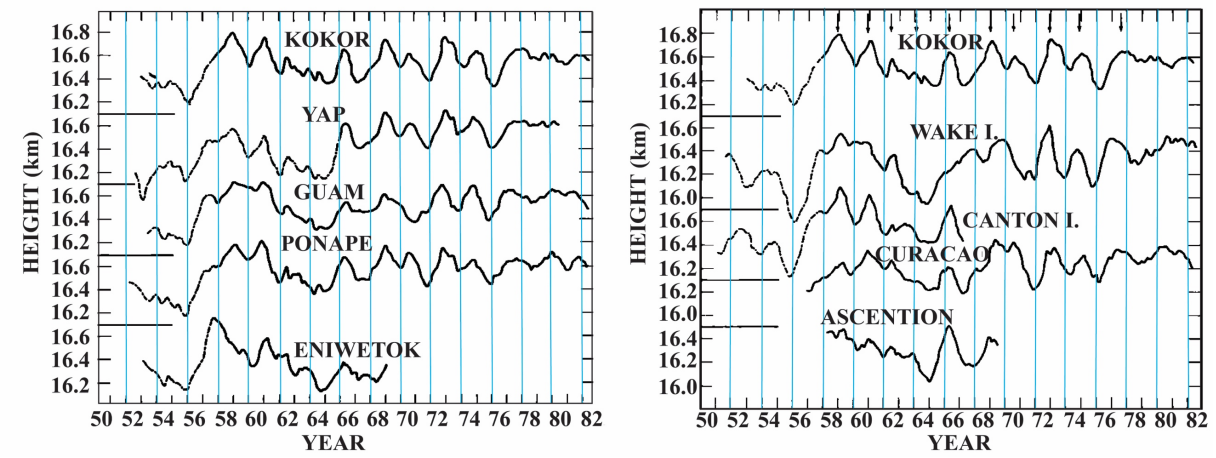

Figure 4. Twelve-month running mean tropopause heights at five Micronesian stations (left panel, after Fig. 2 of Reid and Gage 1985) and for more widely separated stations, including Curacao and Ascension Island in the Atlantic (right panel, after Fig. 3 of Reid and Gage 1985), where arrows at the top identify peaks that occur at more than one station. The 16-km level is indicated for each curve at left. Thin blue vertical lines were added at the beginning of each even year.

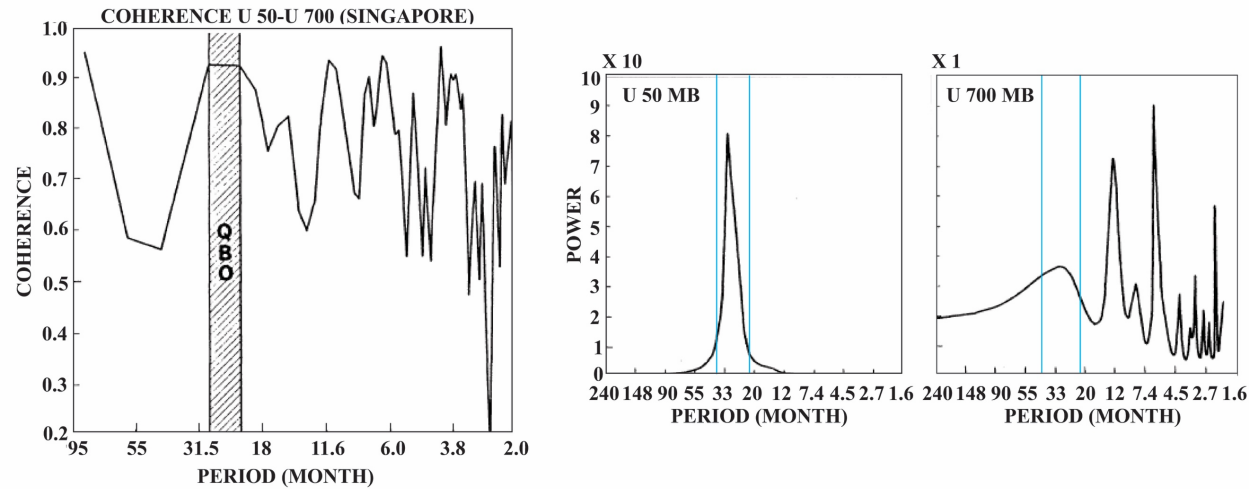

Figure 5. Left: coherence spectrum of monthly mean zonal wind between 50 and 700 hPa at Singapore. Right: individual power spectra at 50 and 700 hPa for the 18-yr period 1963-1981. Power spectrum units plotted are in m/s per month and a maximum lag of 40 was used. Note that the power scale for 50 hPa is 10 times that for 700 hPa. Thin blue vertical lines were added to the power spectra to highlight the band ~22-36 months (adapted from Fig. 3 of Yasunari 1989).

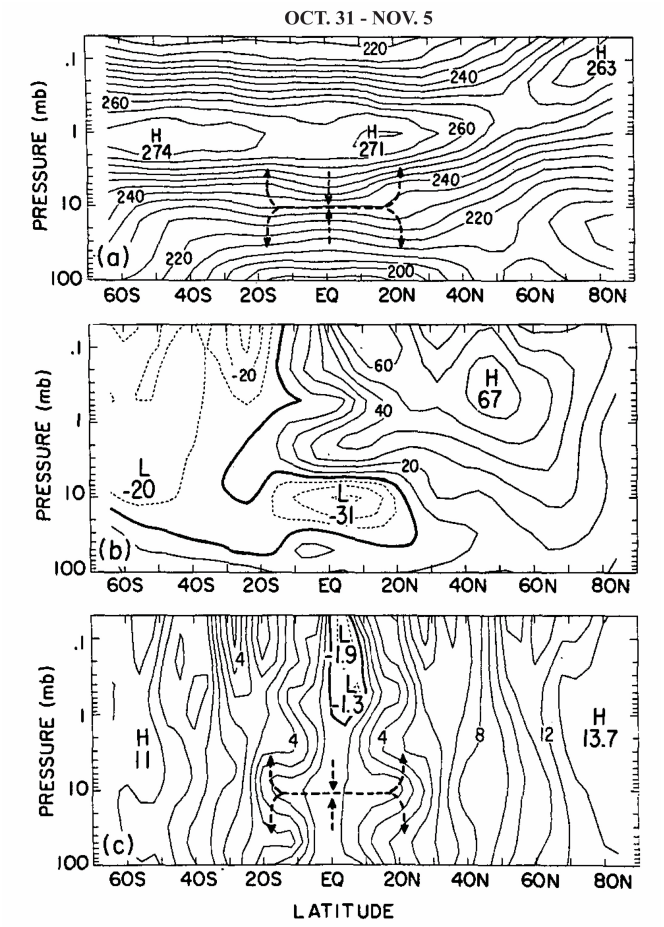

Figure 6. Latitude-altitude sections of zonal mean LIMS a) temperature (contour interval 5 K), b) zonal wind (interval 10 m/s) and c) normalized absolute vorticity (see text, contour interval 1 day^{-1}) for the period 31 October – 5 November 1978. Values of temperature and zonal wind have been smoothed with a 1-2-1 filter in latitude. Schematic arrows indicate the MMC which is compatible with the observed patterns in temperature and PV and with theoretical models. (Fig. 4 of Hitchman and Leovy 1986. © American Meteorological Society. Used with permission.)

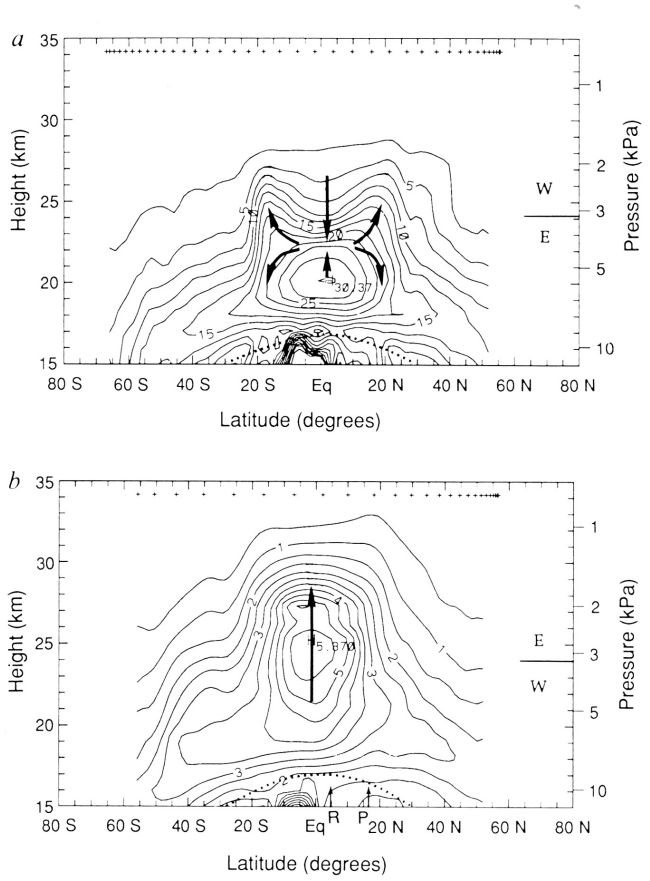

Figure 7. Latitude-altitude sections of aerosol extinction ratio at 1 um during two 40-day periods representative of two different phases of the QBO: a) dominant westerly shear centered at 11 November 1984 (contour interval 2.5) and b) dominant easterly shear, centered at 4 October 1988 (contour interval 0.5). Crosses indicate locations of the daily average of ~15 profiles. Arrows indicate the inferred QBO circulation based on the aerosol distribution. The altitude of the zero-wind line at the equator is shown at the right of each section. The tropopause is indicated with a dotted line. The latitudes for the eruptions of Mt. Ruiz in November 1985 and of Mt. Pinatubo in June 1991 are indicated by "R" and "P", respectively, both of which occurred during easterly shear in the lower stratosphere. (Figure 3 of Trepte and Hitchman 1992).

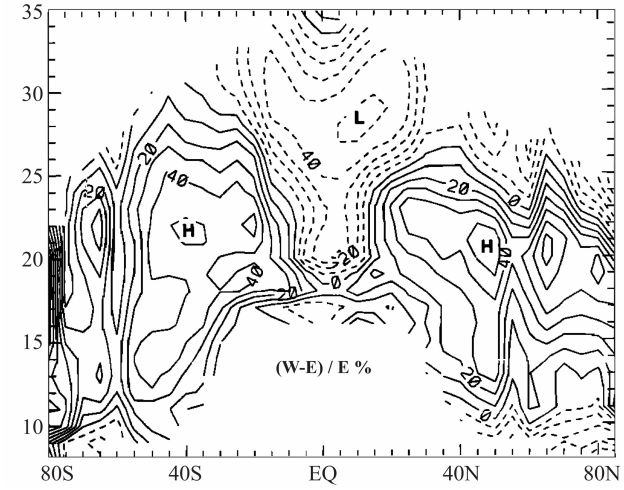

Figure 8. QBO W-E differences in SAGE aerosol extinction ratio (contour interval 5%), using the 50-70 hPa wind shear index, based on 10 years (1979-1981 and 1984-1990) of SAGE I and II and SAM II aerosol measurements. Dashed contours indicate higher aerosol during QBO E shear (Fig. 7 of Hitchman et al. 1994).

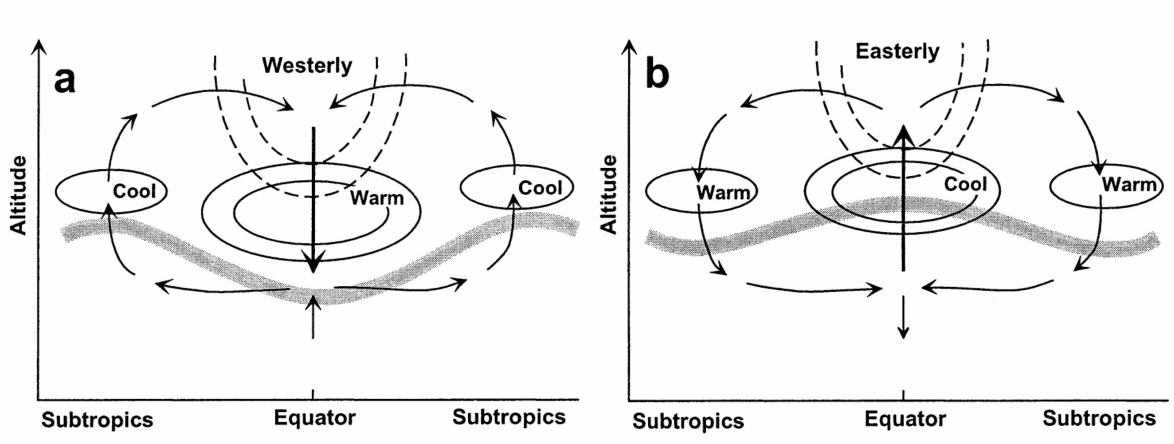

Figure 9. Schematic diagram of the QBO MMC and its relationship with anomalies of zonal mean temperature (solid contours), zonal velocity (dashed contours) and tropopause altitude (thick gray lines) for a) warm anomaly during descending QBO W regime and b) cold anomaly during descending QBO E regime approaching the UTLS (from Collimore et al. 2003, © American Meteorological Society, used with permission. Cf. similar diagrams in Gray et al. 1991b and Trepte 1993).

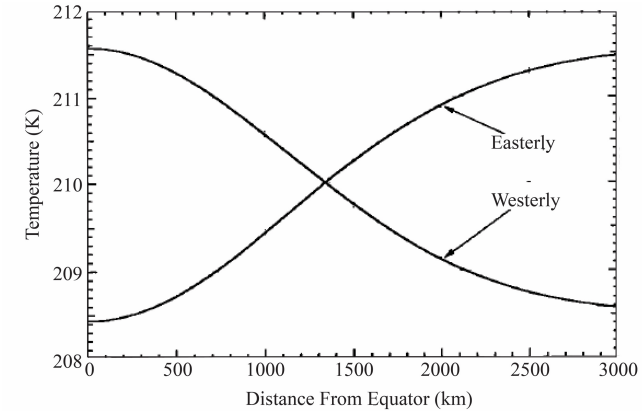

Figure 10. "Calculated temperature anomalies forced by the easterly and westerly phases of the quasi-biennial wind variation." A typical value for vertical shear of 3 m/s per 6 km and a mean equatorial temperature of 210 K were assumed, (Fig. 8 from Reid, 1994).

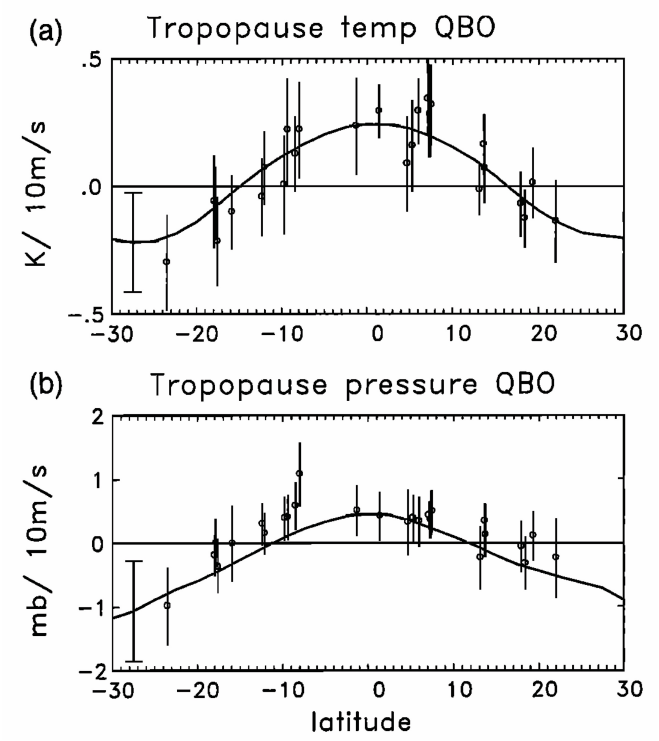

Figure 11. "Latitudinal structure of QBO variations in a) tropopause temperature (K per 10 m/s) and b) tropopause pressure (hPa per 10 m/s) for 1979-1997, derived from regression analysis. Curves show NCEP data, and circles indicate results for each radiosonde location. Error bars indicate +/-2 sigma statistical uncertainties. Units are Kelvins per 10 m/s of QBO winds at 50 hPa, which vary over ~+/-20 m/s during a QBO cycle" (Fig. 13 of Randel et al. 2000).

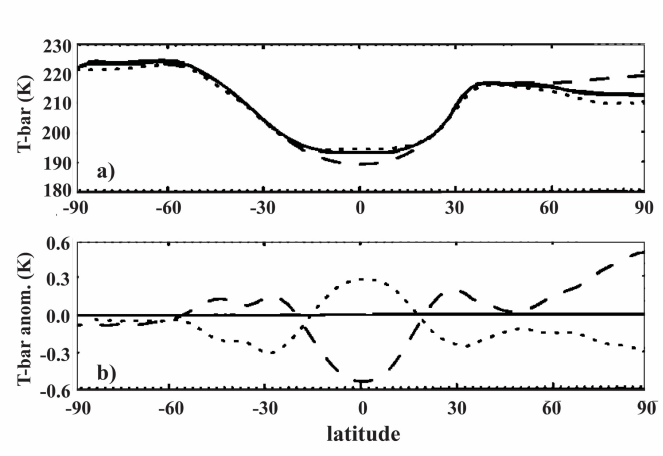

Figure 12. a) Latitudinal distribution of NCEP zonal mean tropopause temperature (K) for DJF QBO W (dotted line), QBO E (dashed line), and climatological mean (solid line). b) QBO W (dotted line) and QBO E (dashed line) departure from the annually averaged zonal mean tropopause temperature (K). Deviations from climatology in a) are exaggerated by a factor of 5 for clarity (Fig. 15 of Huesmann and Hitchman 2001).

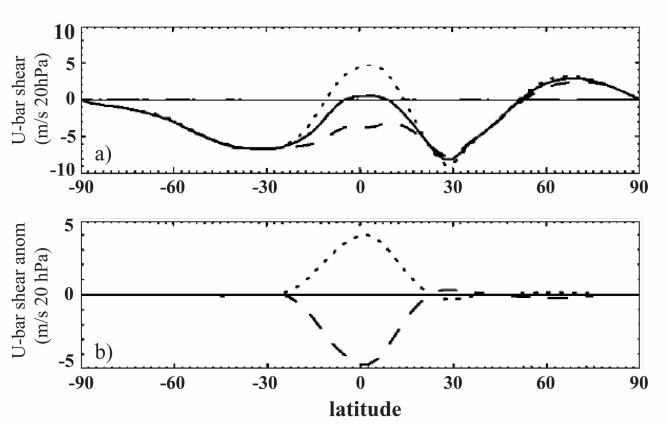

Figure 13. a) Latitudinal distribution of NCEP 50-70 hPa zonal mean wind shear (m/s per 20 hPa) for DJF QBO W (dotted line), QBO E (dashed line), and climatological mean (solid line). b) QBO W (dotted line) and QBO E (dashed line) departure from the annually averaged 50 – 70 hPa wind shear (Fig. 9 of Huesmann and Hitchman 2001).

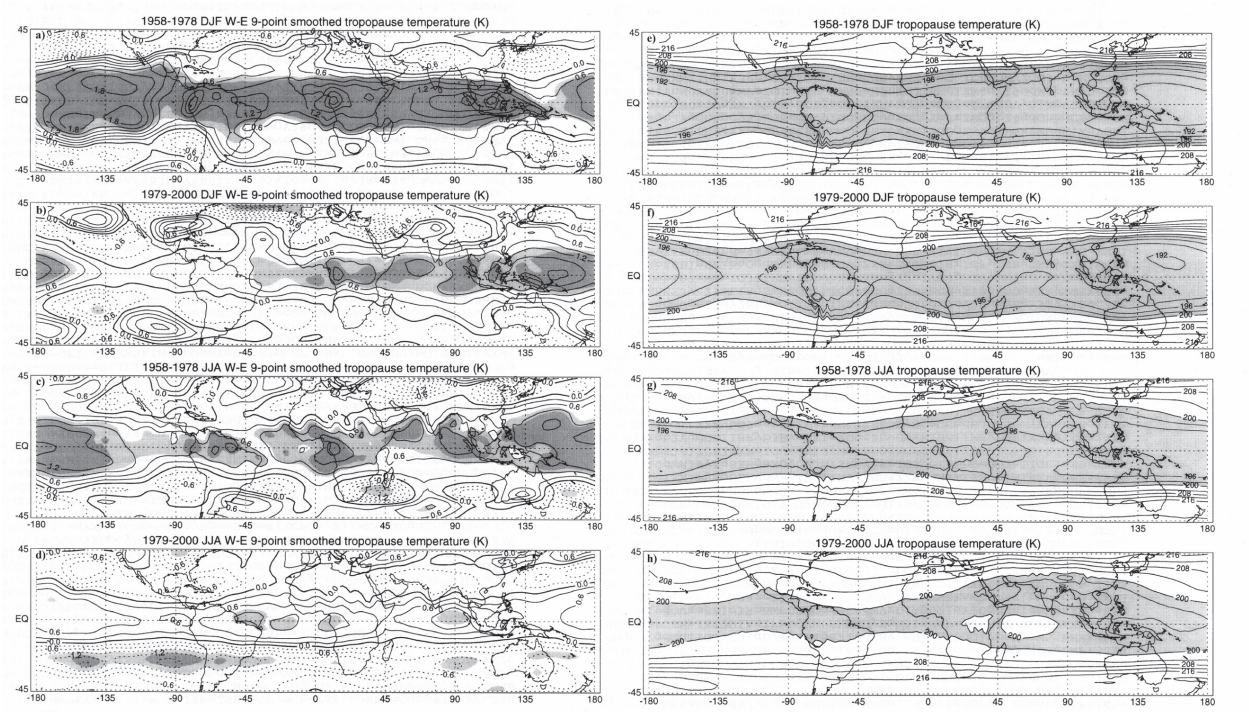

Figure 14. Seasonally-averaged (left, panels a-d): QBO W-E NCEP tropopause temperature (contour interval 0.3 K, dashed contours negative), and (right, panels e-h): NCEP mean tropopause temperature (contour interval 3 K in the shaded regions below 200 K, 4 K elsewhere), for DJF (panels a, b, e, f) and for JJA (panels c, d, g, h). NCEP data during 1958-1978 and 1979-2000 are shown separately for each season (upper and lower of each pair). In the QBO W-E difference fields (left), light shading indicates confidence level above 90%, dark shading above 95%, and the fields have been smoothed once with a 9-point square filter.

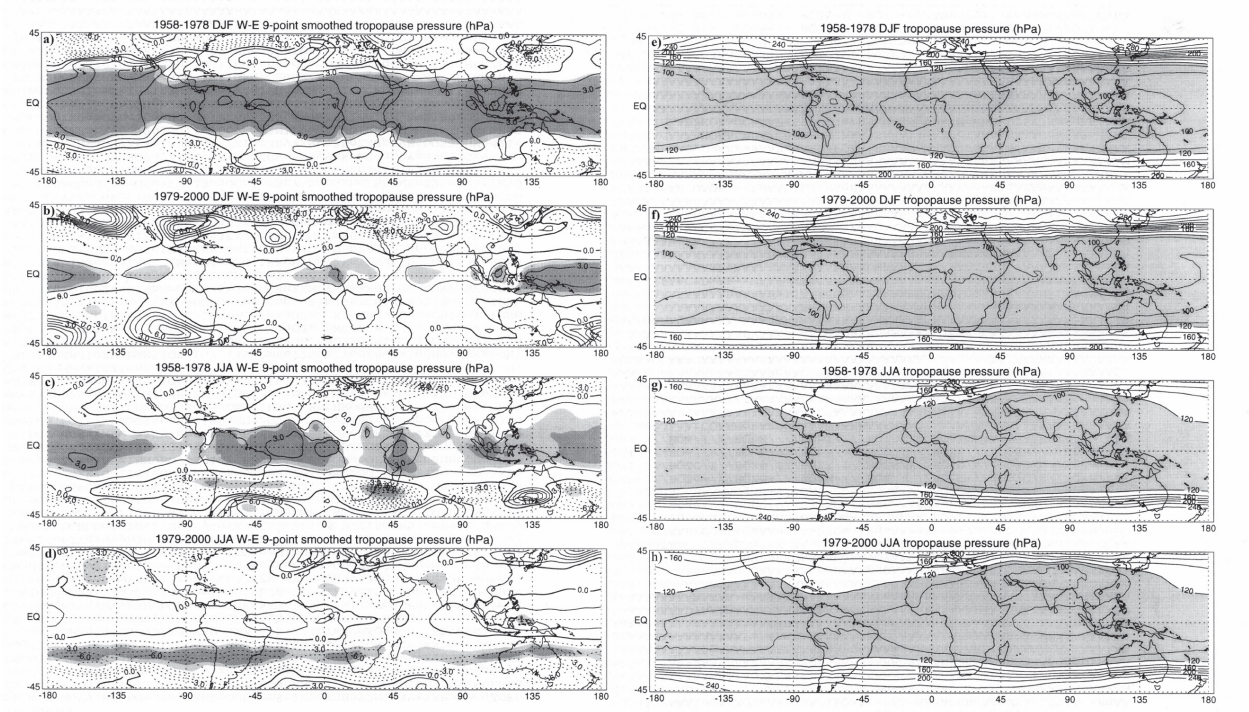

Figure 15. As in Fig. 14, except for NCEP tropopause pressure. In the QBO W-E plots (left, panels a-d), the contour interval is 1.5 hPa, with dashed contours negative, and light shading indicates confidence level above 90%, dark shading above 95%. In QBO seasonal mean plots (right, panels e-h), the contour interval is 10 hPa in the shaded region below 120 hPa, and 20 hPa elsewhere.

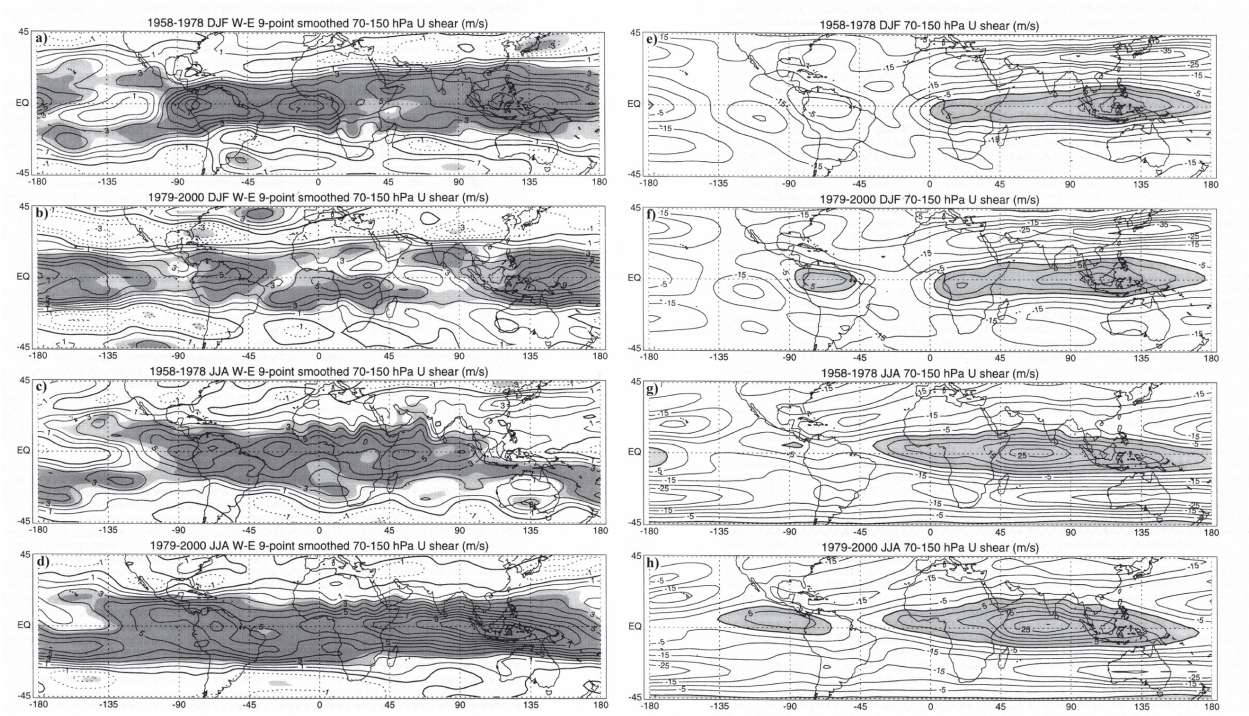

Figure 16. As in Fig. 14, except of NCEP 70 - 150 hPa zonal wind shear. In the QBO W-E plots (left, panels a-d) the contour interval is 1 m s^{-1} $(80\ hPa)^{-1}$, with dashed contours negative, and light shading indicates confidence level above 90%, dark shading above 95%. In seasonal mean plots (right, panels e-h), the contour interval is 5 m s^{-1} $(80\ hPa)^{-1}$, with positive values shaded.

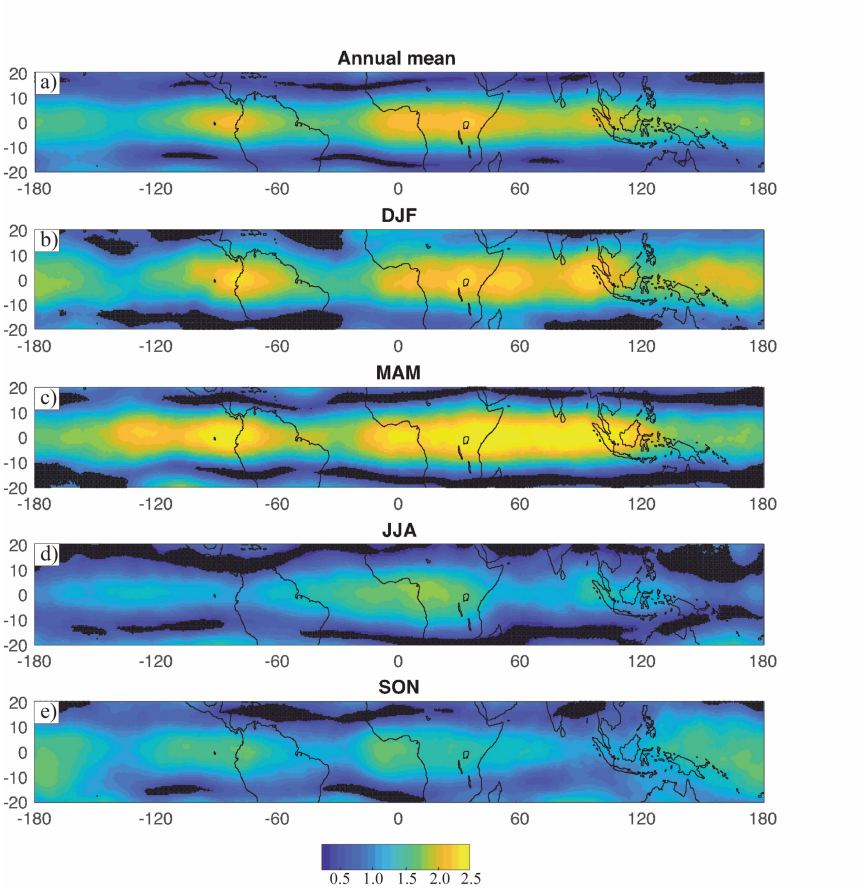

Figure 17. QBO W-E range in MERRA-2 CPT temperature (color bar, contour interval 0.125 K) for the 38-yr period 1980-2017, for a) the annual mean, b) DJF, c) MAM, d) JJA, and e) SON. Regions with less than 99% confidence are indicated in black.

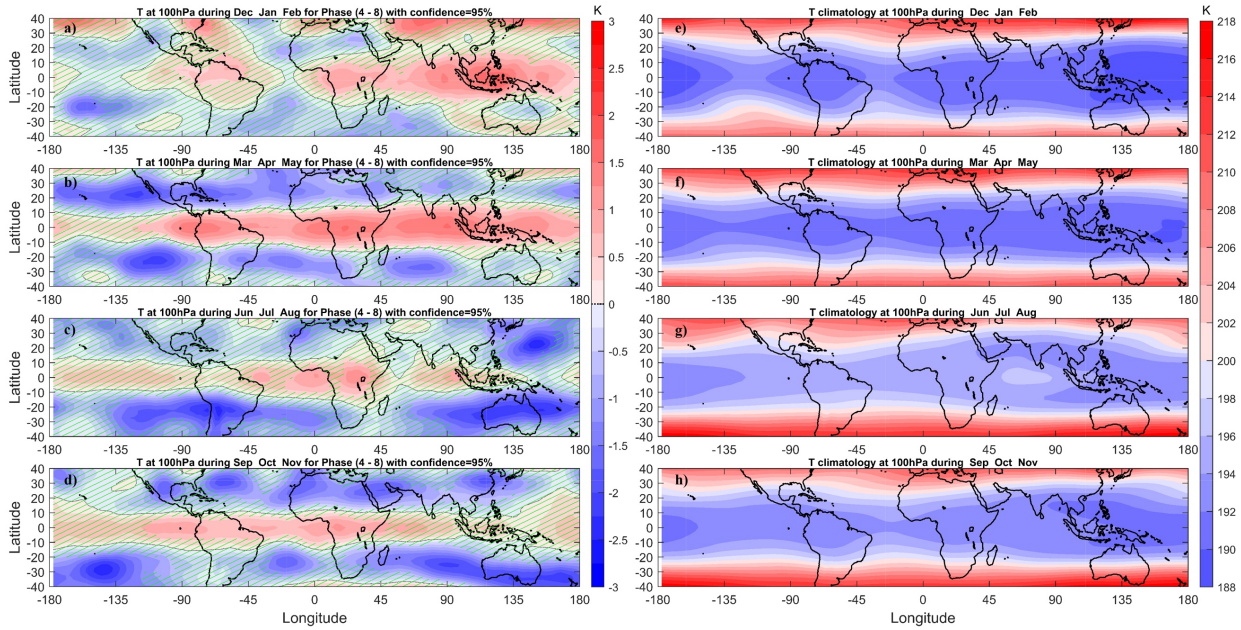

Figure 18. Seasonal mean ERA-Interim 100 hPa temperature (left, panels a-d): QBO W-E differences (color bar, range -3 to 3 K, contour interval 0.25 K), and (right, panels e-h): seasonal means (color bar, range 188 to 218 K, contour interval 2 K), for DJF (a, e), MAM (b, f), JJA (c, g), and SON (d, h). Monthly mean data for the 40-yr period 1979 – 2018 were analyzed using the EOF method of Wallace et al. (1993). QBO W-E values shown are phase-4 minus phase-8, which corresponds W and E maxima in the lower stratosphere. Diagonal green lines indicate regions with less than 95% statistical significance. In the left-hand panels, the zero line, or node, is indicated with a dotted black line.

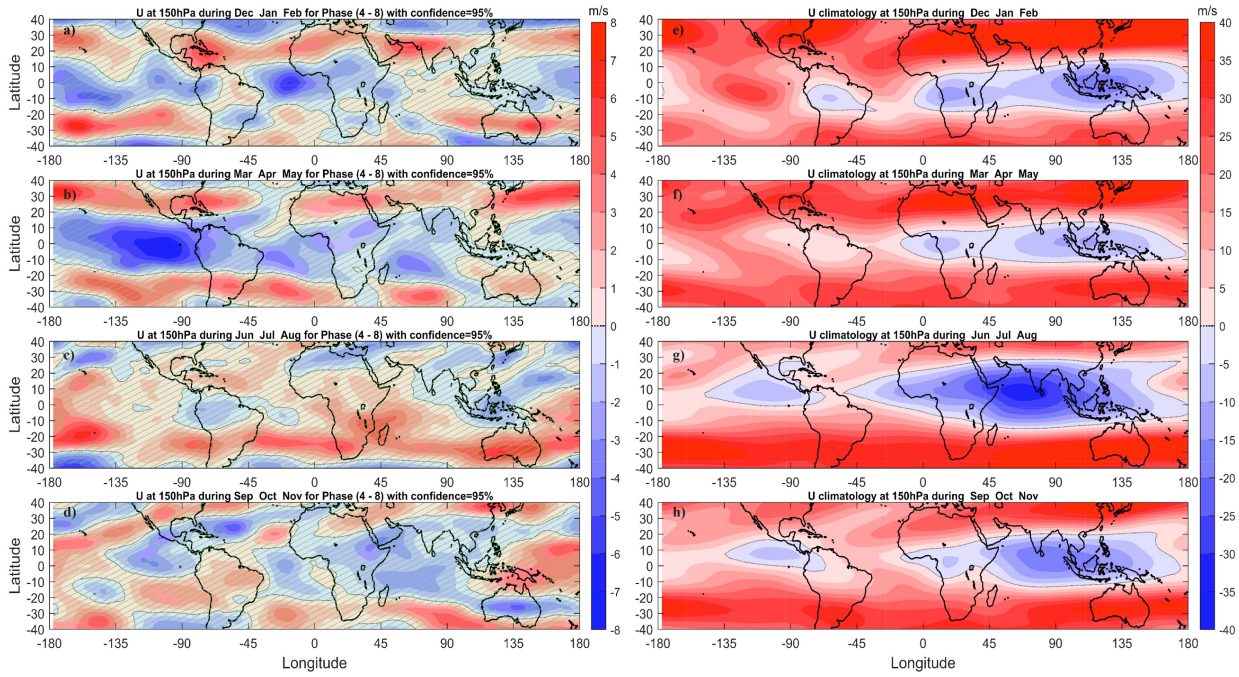

Figure 19. As in Fig. 18, except of (left, panels a-d): QBO W-E differences in 150 hPa zonal wind (color bar, range -10 to 10 m/s, contour interval 1 m/s) and (right, panels e-g): seasonal mean distribution of 150 hPa zonal wind (color bar, range -40 to 40 m/s, contour interval 5 m/s). The zero contour is represented with a dotted black line.

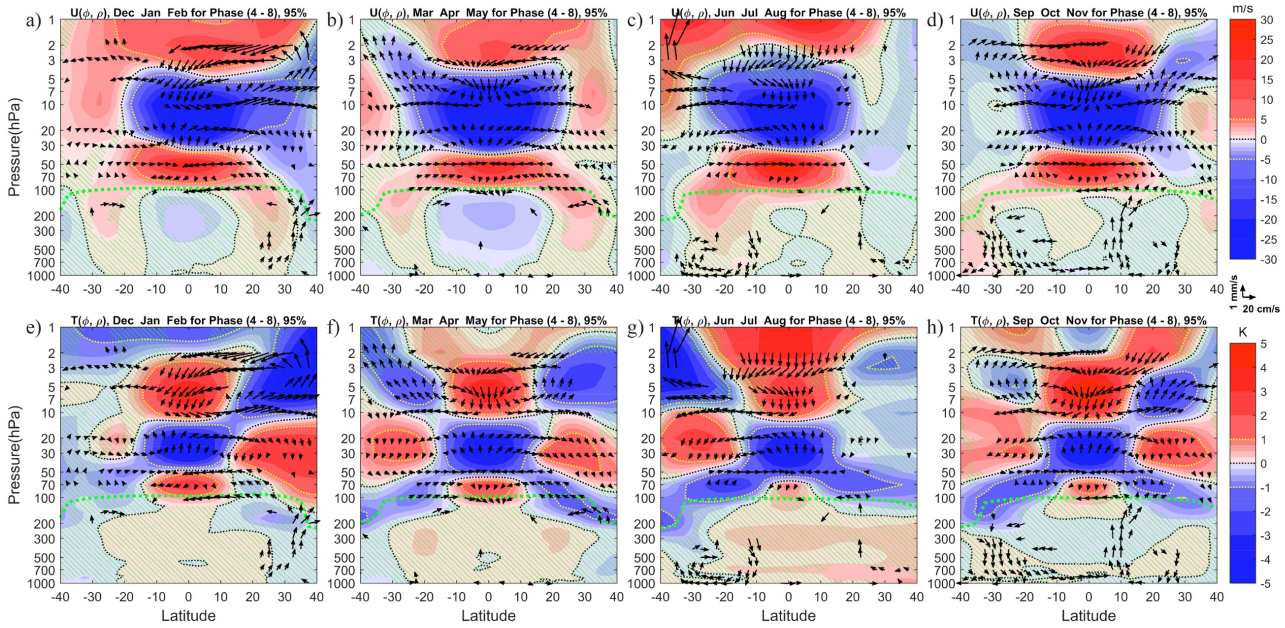

Figure 20. Seasonal mean ERA-Interim zonal mean QBO W-E (phase 4 minus phase 8 differences) data for DJF (a, e), MAM (b, f), JJA (c, g), and SON (d, h), in the domain 0-50 km (1000 -1 hPa), 40°S-40°N, of (a-d) zonal wind (color bar, range -30 to 30 m/s, with contour interval 1 m/s until +/-5 m/s, and an interval of 5 m/s for larger values), and (e-g) temperature (color bar, range -5 to 5 K, interval 0.25 K until +/-1 K, and an interval of 1 K for larger values). Reference vector scales of 1 mm/s for vertical motion and 20 cm/s for meridional motion are shown. The black dotted line is the zero contour. The yellow dotted lines separate regions of fine and coarse contour intervals. The heavy-dashed lime green line indicates the seasonal mean tropopause. Monthly mean data for the 40-yr period 1979 – 2018 were analyzed with the EOF method of Wallace et al. (1993). Phases 4 and 8 correspond to QBO W and E maximizing in the lowest stratosphere. Diagonal green hatching indicates regions with less than 95% statistical significance. Vectors are not plotted if both components are not significant at the 95% level.

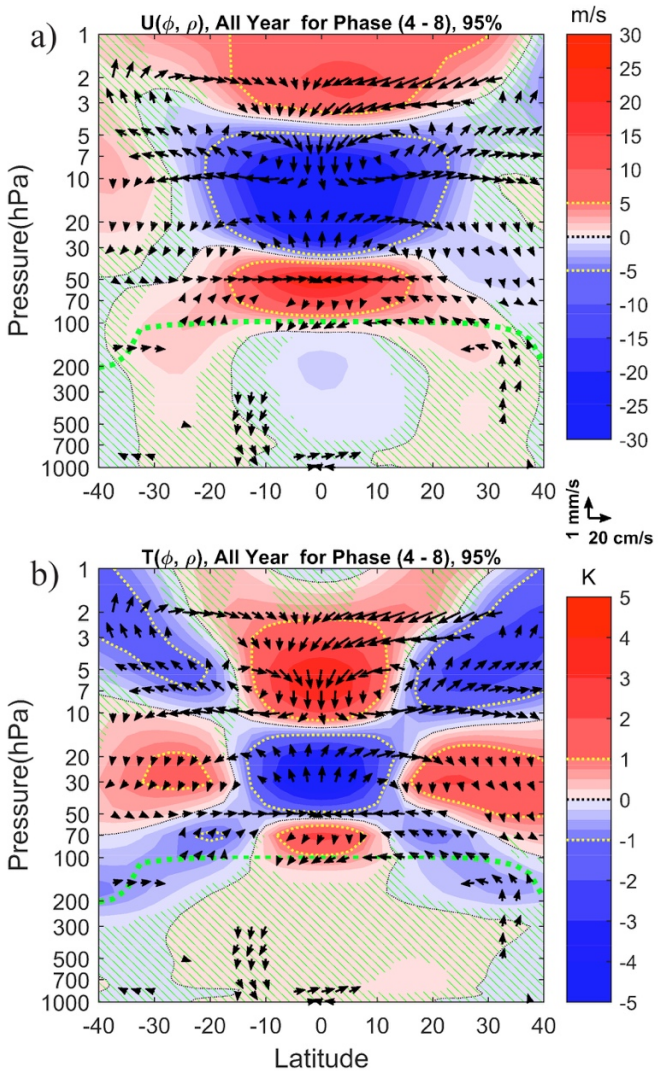

Figure 21. Time mean ERA-Interim QBO W-E differences during the 40-yr period 1979-2018, in the domain 0-50 km (1000 -1 hPa), 40°S-40°N, for a) zonal wind (color bar, range -30 to 30 m/s, with contour interval 1 m/s until +/-5 m/s, with interval 5 m/s for larger values), and b) temperature (color bar, range -5 to 5 K, interval 0.25 K until +/-1 K, with interval 1 K for larger values). The reference vector scales of 1 mm/s for vertical motion and 20 cm/s for meridional motion are shown. The black dotted line is the zero contour. The yellow dotted lines separate regions of fine and coarse contour intervals. The heavy-dashed lime green line indicates the time mean tropopause. Monthly mean data were analyzed with the EOF method of Wallace et al. (1993). Phases 4 and 8 correspond to QBO W and E maximizing in the lowest stratosphere. Diagonal green hatching indicates regions with less than 95% statistical significance. Vectors are not plotted if both components are not significant at the 95% level. A climatological mean tropopause is indicated with a thick dashed gray line (~100 hPa in the tropics and ~250 hPa near 40°).